

# **The beginning of a new era in bone surgery**

## **Effectiveness and clinical application of a cold-ablation and robot-guided laser osteotome**

**Inauguraldissertation**

zur

Erlangung der Würde eines Dr. sc. med

Vorgelegt der

Medizinischen Fakultät

der Universität Basel

von

Marcello Augello

aus Münchwilen (TG)

Basel, 2020

Originaldokument gespeichert auf dem Dokumentenserver der Universität Basel

**[edoc.unibas.ch](https://edoc.unibas.ch)**

Genehmigt von der Medizinischen Fakultät  
auf Antrag von

Prof. Dr. Oliver Bieri  
*Prüfungsvorsitz und Fakultätsverantwortlicher*

Prof. Dr. Dr. Philipp Jürgens  
*Dissertationsleiter*

Prof. Dr. Philippe Cattin  
*Co-Dissertationsleiter*

Prof. Dr. Dr. Sylvie Testelin  
*Externe Expertin*

Basel, 2020

Prof. Dr. Primo Leo Schär  
Dekan der Medizinischen Fakultät

Meinen Eltern  
in Liebe und Dankbarkeit.

## Acknowledgments

A scientific paper is rarely the sole achievement of one individual. Rather, in addition to the scientific framework, those decisive are people who you encounter as a doctoral student on your path. There are the ones who actively support and the others who without realizing it make a valuable contribution, maybe only through a word or an encouraging smile. In the following, I would like to thank the people who, in one way or another, have contributed to my graduation.

Firstly, I would like to thank Professor Hans-Florian Zeilhofer, who encouraged me to start with the PhD. Additionally, he gave me the possibility to connect with the scientific teams that I needed to realize this project.

Secondly, my special gratitude goes to my co-supervisors, Professor Philipp Jürgens and Professor Philippe Cattin, whose critical feedback of my experiments kept me on track, and whose prompt and kind replies to all my questions helped me to stay every time optimistic. Both of you gave me the crucial support I needed for my publications with important inputs to fulfill my PhD.

My thanks also go to all members of the PhD board of the Department of Biomedical Engineering, and in particular, its head, which enabled me as a clinician the opportunity and the trust to conduct this PhD project.

I am also very grateful, and I acknowledge the Advanced Osteotomy Tool AG team for the great cooperation all these years. Above all, thanks for the support received during the prototype testing phases. In particular, I would like to thank Alfredo and Cyrill

Many thanks go to the team of the veterinary faculty of the animal hospital in Zurich for the wonderful support during the animal study, and especially to Dr. Katja Nuss.

I also offer my thanks to Professor Magdalena Müller-Gerbl and the anatomical dissectors, Peter Zimmermann and Roger Kurz, who supported this work from a very early stage, at a time when the preliminary results were lacking, and research questions were vague. Thank you for this great trust.

Thanks to my friends for their understanding and motivational words. You are the best! To my parents and my wife, my biggest thanks, which I cannot express with words. I admire them for their courage and their strength to let me go my way and support me in every decision.

Finally, I thank all the people not mentioned above but very important to me for the realization of this thesis.

## Summary

Most industrial laser applications utilize computer and robot assistance, for guidance, safety, repeatability, and precision. For industrial applications, the increase in throughput and the processing speed are in the foreground. Nevertheless, these tools cannot just be transferred into clinical and surgical use because the focus in surgical interventions is on the exact implementation of a unique plan. The patient, as an inaccurately defined workpiece, with its individual anatomy and pathology, ultimately needs a single lot planning. Nowadays, medical laser systems are hand driven. The possibility of working precision, as used in industry lasers, is not exhausted. Therefore, medical laser beams have to be coupled to robot guidance. But due to the over-size of commercially available tools, efficient and ergonomic work in an operating room is impossible. Integration of the systems such as the laser source, and the robot arm are needed. Another key issue for the accuracy of the robotic arm is the inclusion of a tracking system. All these issues were encountered developing CARLO®: a Cold-Ablation and Robot-guided Laser Osteotome.

This PhD thesis is divided in three parts:

- an in-vivo study in sheep,
- an in-vitro / wetlab study on human cadavers, and
- a theoretical-experimental study to evaluate biomechanical changes in different osteotomy pattern.

To test the applicability of the system in an operation theatre similar environment, an in-vivo animal trial was performed. Additionally, we wanted to demonstrate that bone healing after laser osteotomy is not impaired compared to the standard tool the piezo-osteotome. In terms of new mineralized bone formation, histological and micro-CT analysis showed clearly a higher tendency towards the acceleration of the healing process in the laser group. Additionally, no signs of bone necrosis were seen.

In addition to the pure functioning of the device, the applicability in the clinic is important for technology to prevail. Therefore, dummy tests for the ergonomics and cadaver tests for the simulation of "real" operations in the cranio-maxillofacial field were performed. Wetlab tests were conducted on human cadavers where different macro-retentive osteotomy patterns were performed. It could be demonstrated that our prototype shows advantages over the current state of the art cutting tools, e.g. reduced bone loss, precise and real-time navigated execution of predefined geometries of freely selected osteotomy patterns. This advantage can be

implemented in another indication of our prototype in the cranio-maxillofacial field: in craniosynostosis surgery. We performed a study using finite element analysis to simulate incomplete osteotomies on the inner side of the bone flap to facilitate the re-shaping (skull molding). This biomechanical analysis intended to create basic knowledge in terms of the best stress vs. force relation to obtain the largest projected bone surface.

Moreover, a human multicenter study is ready to start for the clinical introduction of the cold-ablation and robot-guided laser osteotome and to gain more experience and information for future work.

## Zusammenfassung

Die meisten industriellen Laseranwendungen nutzen Computer- und Roboterunterstützung, um Führung, Sicherheit, Wiederholgenauigkeit und Präzision zu gewährleisten. Für industrielle Anwendungen stehen die Durchsatzsteigerung und die Prozessgeschwindigkeit im Vordergrund. Trotzdem können diese Werkzeuge nicht einfach in die klinische und chirurgische Anwendung übertragen werden, da bei chirurgischen Eingriffen die genaue Umsetzung eines einzigartigen Plans im Mittelpunkt steht. Der Patient benötigt als ungenau definiertes Werkstück mit seiner individuellen Anatomie und Pathologie letztendlich eine einzige Planung. Dadurch wird die erreichte Ausführungsgenauigkeit gegenüber den Industrielasern reduziert. Medizinische Laserstrahlen müssen an die Roboterführung gekoppelt werden. Aufgrund der Übergrösse handelsüblicher Geräte ist ein effizientes und ergonomisches Arbeiten im Operationssaal nicht möglich. Es erfordert eine Integration der Systeme, d. h. der Laserquelle und des Roboterarms. Ein weiteres wichtiges Thema für die Genauigkeit des Roboterarms ist die Einbeziehung eines Trackingsystems. Alle diese Probleme wurden mit der Entwicklung von CARLO® angegangen: Ein kalt-abladierendes und robotergeführtes Laser Osteotom.

Diese Doktorarbeit ist in drei Teile gegliedert:

- eine In-vivo-Studie mit Schafen
- eine In-vitro / wetlab-Studie an menschlichen Kadavern und
- eine theoretisch-experimentelle Studie zum zur Evaluation biomechanischem Verhalten bei unterschiedlichen Osteotomie-Mustern.

Um die Anwendbarkeit des Systems in einer dem Operationssaal ähnlichen Umgebung nachzuweisen, wurde ein Tierversuch in vivo durchgeführt. Darüber hinaus wollten wir zeigen, dass die Knochenheilung nach Laserosteotomie im Vergleich zum Standardwerkzeug dem Piezo Osteotom nicht beeinträchtigt wird. In Bezug auf die Bildung von mineralisiertem Knochen zeigten die histologische und die Mikro-CT-Analyse eine deutlich höhere Tendenz zur Beschleunigung des Heilungsprozesses in der Lasergruppe. Ausserdem wurden keine Anzeichen einer Knochennekrose beobachtet.

Neben der reinen Funktion des Geräts ist die Anwendbarkeit in der Klinik wichtig, damit sich eine Technologie durchsetzen kann. Daher wurden im Wetlab Dummy-Tests für die Ergonomie- und Kadavertests für die Simulation "realer" Operationen im Bereich der Mund-,



Kiefer- und Gesichtsheilkunde durchgeführt. Es wurden verschiedene makroretentive Osteotomiemuster in Ober- und Unterkiefern durchgeführt. Es konnte gezeigt werden, dass unser Prototyp Vorteile gegenüber dem Stand der heutigen Tools aufweist, z. B. weniger Knochenverlust, präzise und in Echtzeit navigierte Ausführung von vordefinierten Geometrien von frei gewählten Schnittmustern.

Dank der freien Wahl an verschiedenen Schnittmustern sehen wir eine weitere Einsatzmöglichkeit des Prototyps in der Craniosynostose Chirurgie. Wir führten eine Finite Element Method Untersuchung durch, um unvollständige Osteotomien auf der Innenseite eines virtuell rekonstruierten Knochendeckels zu simulieren, um die Verformung des Knochens zu erleichtern. Mit diesen biomechanischen Analysen wurden Grundkenntnisse über das beste Verhältnis zwischen Belastung und Kraft zu erlangen, um eine beste mögliche Vergrößerung der projizierten Knochenoberfläche zu erhalten.

Schlussendlich steht eine multizentrische Studie am Menschen für die klinische Einführung des Prototyps bereit, um weitere Erfahrungen und Informationen für die zukünftige Arbeit zu sammeln.

# Contents

<b>Acknowledgements</b>	<b>iii</b>
<b>Summary</b>	<b>iv</b>
<b>Zusammenfassung</b>	<b>v</b>
<b>1. Introduction</b>	<b>1</b>
1.1 Hard tissue ablation with laser light	2
1.2 State of the art in laser osteotomy	4
1.3 The need for system integration	6
1.4 The cold-ablation and robot-guided Er:YAG laser osteotome (CARLO®)	8
1.5 Motivation of this PhD-Thesis	10
1.6 Literature	13
<b>2. Pre-clinical in vivo animal test of craniotomy application in sheep model</b>	<b>17</b>
2.1 Comparative microstructural analysis of bone osteotomies after cutting by computer-assisted robot-guided laser osteotome and piezoelectric osteotome: an in vivo animal study	18
<b>3 Wet lab human fibulae osteotomies</b>	<b>31</b>
<b>4 Workflow for using CARLO® for mandibular reconstruction with fibula</b>	
<b>Free flap and midfacial osteotomies</b>	<b>32</b>
4.1 Performing partial mandibular resection, fibula free flap reconstruction and midfacial osteotomies with a cold ablation and robot-guided Er:YAG laser osteotome (CARLO®) – A study on applicability and effectiveness in human cadavers	33
<b>5 The use of FEM analysis for modeling different osteotomy patterns and biomechanical analysis of craniosynostosis treatment</b>	<b>45</b>
<b>6 Discussion and Outlook</b>	<b>62</b>
6.1 Discussion	61
6.2 Outlook	70
6.3 Literature	72
<b>7 List of publications on PhD topics</b>	<b>74</b>
7.1 Peer-reviewed journal publications	74
7.2 Oral presentations	75
7.3 Posters presentations	76
<b>8 Curriculum vitae</b>	<b>77</b>

# 1. Introduction

The archaeological discoveries of human skulls with osteotomies suggest that impressive results have been achieved with primitive tools already. Osteotomies have been performed for thousands of years with mechanical methods for various purposes. The mechanical instruments have evolved over time; however, these were largely based on the archaic mechanical principles. Despite the myriad range of tools for drilling and cutting, these offer limited freedom to the cutting geometry (straight or gently curving lines and symmetric wholes). Furthermore, the friction between the cutting instrument and the material causes thermal damage itself. In bone surgery, this heat-induced damage leads to necrosis of the tissues at the wound edges. (1,2). Excessive production of heat for sustained duration causes severe damage to bony structures, i.e. carbonization, interfering with the physiological healing and compromising post-operative recovery (3). Eriksson and Albrektsson (4) demonstrated that a threshold temperature greater than 47 °C for more than 1 min resulted in significant thermal injury to the bone. Moreover, these authors noted that temperature elevation between 44 °C and 47 °C may already lead to tissue necrosis. Heat generates vaso-occlusion, followed by bone resorption by osteoclastic overactivity in response to vascular injury. This is succeeded by the replacement of bone tissue by the adipocyte instead of osteocyte (5,6). Osteonecrosis is the term used in relation to an avascular injury to the bone, which will result in the death of osteocytes (7). Following a thermal injury to the bone, osteonecrotic changes will affect the bone's ability to regenerate and heal (8). Lastly, the risk of injury to adjacent soft tissues (e.g., neurovascular structures) should never be underestimated. Other typical limitations of mechanical tools are the procedural bone loss due to the minimum necessary diameter of the instrument, the imprecision of the cut due to the torque-moment, which has to be caught by the hand of the surgeon. Moreover, with the broadening of the cuts by the drill diameter, subsequent deposition of metal shavings and bacterial contamination may result.

The ultrasound-driven piezoelectric osteotome was introduced in the 1990s to overcome the above-mentioned shortcomings. However, its cutting tip is still in direct contact with the bone. Additionally, the cutting geometry is limited by the size and shape of the tip in contact with the bone and the condition of the bone itself. There was a need to develop novel technologies to overcome these limitations. The use of laser light seemed to be a convenient option. Processing of material with laser light is widely used in industrial settings. The benefits conferred by this unique energy source include non-contact processing of the target material, lack of friction-induced mechanical stress, or abrasions, improved quality and productivity and feasibility for automation. Therefore, a major research focus was set on technical

improvements of the laser system and on investigations of the biological effects of basic laser-tissue interactions.

## **1.1 Hard tissue ablation with laser light**

After the development of the first ruby laser by Maimann et al. in 1960 (9), ophthalmology was the first subspecialty in medicine to apply this light source clinically. In 1961, Campbell et al. (10) used a confocal laser-transmission system to perform the first retinal laser coagulation. Three years later, Bridges (11) used an argon laser, which offered the advantage of stronger absorption by hemoglobin and melanin. This system enabled effective photocoagulation in a wider spectrum of retinal diseases, including vascular lesions and a variety of maculopathies.

Subsequently, experimental and preliminary research to identify the laser wavelengths suitable for hard tissue ablation started in the early 1960s. Vaporization of enamel with a pulsed ruby laser was reported in 1964 (12). In the subsequent decade, continuous-wave and long-pulsed medical CO<sub>2</sub>-lasers were tested for cutting mineralized tissue. CO<sub>2</sub> laser wavelengths already showed promising results for soft tissue treatment and thus helped drive the demand for laser osteotomy (13,14). However, the pioneering studies by Horch et al. (15,16) revealed serious biological complications associated with this technique; these included greater incidence of necrosis and delayed bone healing compared with conventional mechanical osteotomies. The discouraging results pushed the idea of using laser for bone surgery into the background. What were the reasons for the negative results with the CO<sub>2</sub> laser?

Thermal conductivity is a key parameter as it determines the propagation of the heat generated by the laser. Bony tissue is composed of 67 % inorganic minerals (hydroxyapatite) and 33 % collagen and non-collagenous proteins. The water content in cortical and trabecular bone is 23.5 % and 30.5 %, respectively (17). Both water and hydroxyapatite absorb laser light in the infrared range and exhibit peak absorption coefficients at wavelengths of approximately 10 µm for water and 3 µm for hydroxyapatite, respectively. Absorption of the highly-focused energy of a laser pulse by the bony tissue induces a tissue expansion, which results in locally increased pressure. When the internal pressure surpasses the bone strength, it results in micro-explosions that lead to thermally induced mechanical tissue ablation. The water content in the bone tissue is vaporized and solid tissue fragments are carried away with the vapor during the micro-explosions. These micro-explosions – heat energy transformed into kinetic acoustic energy - are well audible and achieve up to 120 dB in bone (18) and by the kinetic sound-pressure shock wave, called “photoacoustic effect”, ablate the bone by shattering the

hydroxyapatite crystals and disrupting collagen fibers. Since water does not absorb radiation in the visible and UV range of the wavelength spectrum, pulsed lasers in the infrared spectrum have been mostly used to ablate bone. CO<sub>2</sub> lasers have a wavelength of 10.6  $\mu\text{m}$  with an absorption peak in hydroxyapatite (Figure 1). This effect in CO<sub>2</sub> lasers may result in a substantial increase in temperature, which far exceeds the threshold for protein breakdown and leads to coagulation and vaporization of bone elements and eventual necrosis (19,20).

Research conducted in the subsequent decades focused on the identification of alternative lasers for bone ablation. These included UV excimer lasers (e.g., Xenon monochloride or argon fluoride lasers), which cause direct photoablation and ultra-short pulses (picosecond and femtosecond pulse lengths). The emission wavelengths of these laser types were irrelevant since high irradiation caused plasma-induced ablation of bone tissue, which is independent of the absorption rate. In the late 1990s, other comprehensive studies of short-pulsed infrared laser systems with appropriate wavelengths absorbed by biological hard tissue showed the way for successful ablation of bone. Peavy et al. (21) verified that the best bone ablation results are possible with laser systems working at wavelengths of 2.9  $\mu\text{m}$  and 3.0  $\mu\text{m}$  to reach a strong absorption coefficient for water (Figure 1).

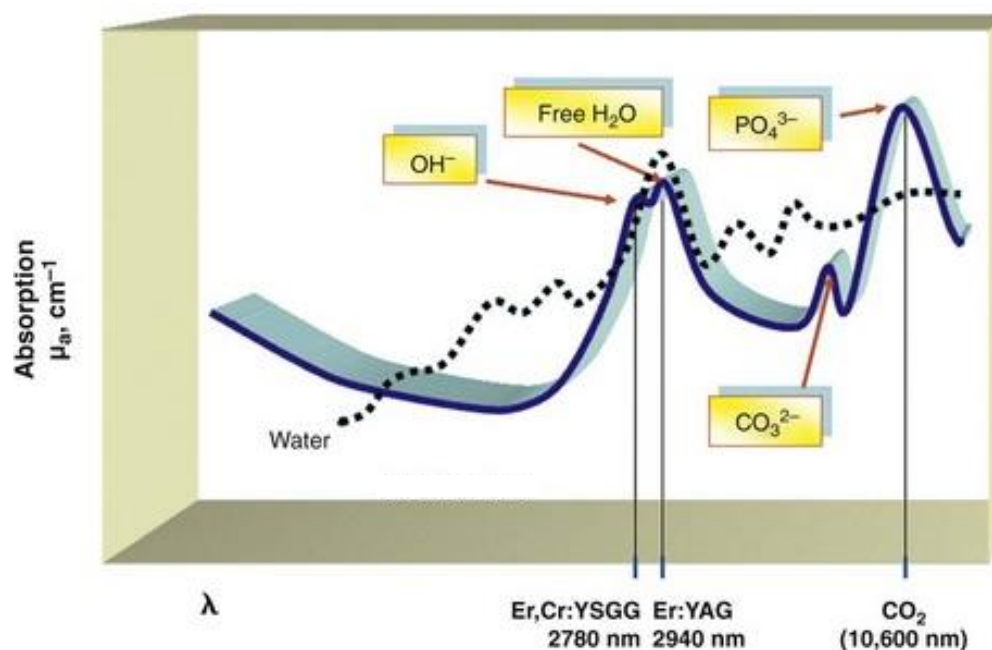


**Figure 1:** Relative absorption of erbium wavelengths in hard tissue chromophores. The absorption peaks represent component radicals of the molecule (hydroxyl, free-water, carbonate, and phosphate). The dotted line represents the absorption of laser energy in water. In contrast the absorption peak for CO<sub>2</sub> lasers is at 10.6  $\mu\text{m}$ .

In this regard, the Erbium-doped Yttrium Aluminum Garnet (Er:YAG) laser system seemed to be the most suitable for the ablation of mineralized tissue (22). Hibst et al. (23,24) demonstrated that mid-infrared laser systems allow an effective and clean thermo-mechanical ablation process. The results show that if the target tissue strongly absorbs laser light and pulse durations were lower than the thermal relaxation time of the tissue, ablation was possible with an acceptable level of thermal damage (25). Choi et al. assumed that the thermal relaxation time for bone is best estimated at a range between 20  $\mu$ s and 80  $\mu$ s (26). Majoran et al. (27) found that heat diffusion for Er:YAG lasers at a short pulse lengths (50-300  $\mu$ s) is negligible. Gholami et al. (28) confirmed the minimal temperature rise using an Er:YAG laser. They demonstrated that on the bone irradiated area, the maximum temperature rise was 0.8 °C and 1.6 °C for two different energy peaks, 200 mJ and 400 mJ respectively. These values were measured at a distance of 1.2 cm from the point of irradiated areas for 200 mJ laser while it was 1.5 cm for 400 mJ laser. Thus, the pulse durations one of the goals to control the extent of collateral damage during laser irradiation; the faster the pulse, the lesser is the time available for heat dissipation into adjacent tissues. Other papers confirmed the absence of thermal-induced bone damage using an Er:YAG laser source (29-31). Additional adequate water cooling may dramatically reduce the incidence of tissue necrosis and charring.

## **1.2 State of the art in laser osteotomy**

Since the introduction and initial use of the laser in the 1960's, a wide range of laser sources with different wavelengths of radiant energy has been tested for various indications such as coagulation and ablation of hard and soft tissues. The application of laser systems is profitable when they offer new therapeutic possibilities in contrast to conventional mechanical methods. As already described, after the initial euphoria, the CO<sub>2</sub> laser fell into oblivion due to the carbonization of bony tissue. However, due to the increasing demand for a reliable substitute for mechanical instruments such as chisels, oscillating saws or drills, there was an increasing urgency, especially in the oral and maxillofacial surgery field for the development of more elaborate, accurate and vibration-free bone cutting techniques (32). Numerous scientific-experimental publications (33-37), as well as occasional clinical work (38,39) in international literature, showed that the laser achieved good ablation results for hard and soft tissues.

The benefits of lasers have become well documented over the past years in dentistry. Mainly in oral surgery, the laser light is usually delivered to the hard tissue via a sapphire tip that is manually guided by the surgeon. Nevertheless, the laser provided an alternative to conventional drilling and filling, while often allowing a dentist to use the handpiece driven laser

source to complete procedures (e.g., extensive alloy preparations) without the need for local anesthesia. Many authors demonstrated, that the Er:YAG laser has the ability to ablate hard tissues (bone, dentin, enamel), especially dental implantology and osteotomy were promising applications (40-43).

The use of the laser remained limited as the means to directly determine the distance to critical structures such as blood vessels or nerves is limited. Rupprecht et al. (44) evaluated as first authors a special feedback system to control laser drilling of cortical bone with an Er:YAG laser (energy density, 450 mJ/mm<sup>2</sup>) under water spray cooling. Laser ablation of organic tissue is characterized and accompanied by different acoustical, optical, and thermal signals. The signals can be detected by different sensor systems to control the laser process and to cut tissue without damaging adjacent structures. Assisted by the sensor-based feedback system, a tissue-specific cutting was demonstrated in rabbit femurs and minipig jaws, with ablation rates between 20 and 60 µm/pulse. This could be achieved because the detected signals changed in a characteristic way after the cortical bone layer had been passed. The specimens were evaluated histomorphometrically for the depth of the ablation. A depth equal to 100 % was set relative to the cortical layer. They revealed a mean ablation rate of cortical bone of almost 99 %. Microcomputer tomography evaluation confirmed highly precise and efficient bone ablation that was limited to the cortical bone but did not affect the underlying cancellous bone. They concluded that penetrating the cortical bone layer; the laser beam was promptly interrupted due to the extreme changes of the signal character received by the sensor system. However, due to the missing depth control, laser osteotomy is still assessed to be inferior to other bone cutting techniques like drills or the piezoelectric osteotome. Even though the contact-free mode is highly beneficial for precise and arbitrary cut geometries, the lack of tactile feedback is a restriction of the manual skills and experience of the surgeon. Therefore, the control of an accurate bone removal depth is difficult. An only visual inspection enables the surgeon to assess and guarantee a certain amount of tissue volume ablation and depth.

Stopp et al. (45) concentrated on the creation of defined geometries by navigated laser ablation based on volumetric 3-dimensional data. Here, the laser was used hand-guided and the required accuracy was supposed to be reached by supporting the surgeon with a navigation method. On the basis of computed tomography data, cylindrical cavities in bovine bone were planned with the help of a navigation system. The position of the laser handpiece was optically tracked and the distance to the bone surface was calculated. The authors applied a focused Er:YAG laser without a special scanner system. On the basis of a special mathematical model, theoretical cavity depth for each single laser pulse was calculated and visualized by the navigation system. Continuous material removal was determined in a volume

model. The system allowed visualizing the laser ablation process with an error of less than 1 mm. As main problem in this experimental trial, the authors discussed that only a planar positioning system was used. In a clinical environment, the laser would be operated manually which would definitely complicate the practicability of the system. The authors already reported that they had difficulties to adjust the laser freehand based on the visualized navigation data. A further limitation of the tested model is the assumption that the tissue properties are constant and homogeneous. They concluded that although laser ablation of mineralized tissue is characterized by the removal of an almost fixed amount of material per laser pulse, a clinically determinable control of cutting depth by calculating the ablated bone volume using a volume model with single-volume elements of bone is hardly feasible.

Thus, the limiting factors for a routine application of lasers for bone ablation were the technical drawbacks like the difficult and safe guidance for the laser beam in a combination of missing depth control.

### **1.3 The need for systems integration**

Narrow incisions of only a few hundred microns and free form of geometrically complex bone cuts necessitate precise guidance and targeting of the laser beam. Moreover, the complex 3-dimensional anatomy and the proximity of vulnerable structures call for a high degree of precision and accuracy. Hence, the integration of this new cutting technology with computer and robot-assisted surgery is indispensable. Indeed, fast and accurate deflections of the laser beam with a beam scanner and its positioning by a robotic system have been used in industrial applications for cutting and welding materials. In addition, the oversize of these devices is not appropriate. The experience from the industrial application of lasers for robot-assisted machining of workpieces cannot be transferred to the medical context. The patient, as an inaccurately described workpiece and the inter-individual variability in anatomy and pathology necessitates a single-piece production. Widespread integration of fixed motion sequences in industrial applications is, therefore, out of question. While industrial applications focus on increasing throughput and process speed, surgical intervention focuses on the exact implementation. The most challenging aspect is to provide an appropriate operative system and to develop the means to implement such an integrated system in the operation theatre. However, usability remains a significant limiting factor. Clinical application of laser osteotomy would require considerable downsizing of the entire laser-robot system. Furthermore, the integration of a robotic system in the operating room requires careful consideration from the perspective of risk management. Various technologies have been introduced in medicine, but not all can be used clinically due to the large size of the tools.



Different research groups have spent efforts on this topic. To mention is the group around Burgner (46). Here short-pulsed CO<sub>2</sub> laser pulses were delivered through a passive articulated mirror arm to a 2-dimensional computer-controlled beam deflector. The beam deflector was coupled as an independent tool to the robot flange. Thus, in addition to the tracking camera for the navigation system three bulky devices were needed disturbing a proper surgical workflow (e.g. obstruction of space or the view of the surgeon).

Another group that dealt with this topic was Jivraj et al. (47). Here a pattern, which represented an osteotomy trajectory, was detected by an optical system. This in-house surgical navigation system consisted of a stereoscopic, projector-based structured light acquisition system and an infrared tool tracker mounted on a surgical light arm as usually used in the operation room. In this way, the tracking system was similarly positioned above the surgical field to that of a standard surgical light. After processing of the pattern by software, cartesian position and pose information for the robot to follow the trajectory, were generated. On this medical light arm robot, an optical payload with focusing optics and a planar fiducial tracking frame were mounted. Based on these data, the laser-robot system could run the original pattern with high accuracy. In this study, both the robot arm and the optical/laser system could be downsized, but above all, the optical payload is still bulky for an operating field. The idea that the navigation system was integrated into the surgical lamp is beneficial. In reality, the tracking field is constantly disturbed by the heads of the surgeons and by the repeated adjustment of the light angle for an optimal illumination of the operation site.

The study of Brandmeir et al. (48) demonstrated also encouraging results with a robot-assisted stereotactic system tested on sixteen patients with 117 different trajectories for a neurosurgery purpose. This system consisted of a robot arm with six degrees of freedom with assisted navigation to visualize surgeons' instruments in real-time on the patient images (these are CT scans or magnetic resonance images). Advantageous of this robot system was its miniaturization like a C-arm. No laser ablating system was integrated so that the borehole osteotomy of the skull was performed with a mechanical instrument.

In summary, to date, no system offers good usability of a miniaturized ablating laser system with robotic guidance to perform osteotomies autonomously, to a level that allows optimal access for the surgeons' staff to the surgical site. Obviously, such a system has to be coupled to a real-time navigation system.

## 1.4 The cold-ablation and robot-guided Er:YAG laser osteotome (CARLO<sup>®</sup>)

The prototype CARLO<sup>®</sup> is a cold-ablation and robot-guided laser osteotome that satisfies the above-mentioned criteria.

It consists of the following five main physical components:

- A tactile medical lightweight robot arm mounted on
- a trolley, housing the computer, the cooling system, and main electronics,
- a custom-made miniaturized Er:YAG laser head mounted at the distal end of the robot containing several opto-mechanical and electronical components, including the ablation laser source,
- an external tracking camera, as a component of the CARLO<sup>®</sup> navigation system, to monitor the real-time position of the navigation markers attached to:
  - a) the pointer tool (with passive markers)
  - b) the patient (with passive markers) and
  - c) the laser head (with active markers)

Various commercially available planning software tools facilitate the widespread adoption of computer-assisted planning. In summary, the process starts with image acquisition where computer tomography slices of the anatomical region are acquired. Based on these data a 3D-model of the region of interest is generated with a high image resolution. Hence, vulnerable anatomical structures such as nerves, vessels or teeth roots can be spared. After the virtual planning of the osteotomy pattern, the cut-out bone segment can be moved. If the surgeon is satisfied with the simulated result of the planned intervention, he can pass the operation plan to the executing unit CARLO<sup>®</sup>.

The class IV Er:YAG ablation laser is held and guided by a seven-axis medical robot [KUKA<sup>®</sup> Light Weight medical-grade Robot (LBR MED), Germany], which is controlled by a navigation system. The joint ranges provide  $\pm 170^\circ$  or  $\pm 120^\circ$  (joint dependent) of movement. The robot is equipped with moment sensors that register unpredicted and dangerous contacts between robotic structures and humans. In case of a collision of the robotic arm with the surrounding environment with a delivered force of  $\leq 65$  N a stop of any device activity, such as laser ablation, is triggered.

The laser source is an Er:YAG laser ( $\lambda = 2.94 \mu\text{m}$ ) that is integrated with an optical system in a compact casing and mounted on the surgical robot. The Er:YAG laser provides a cutting width of  $500 \mu\text{m}$ . The tissue being photoablated is permanently cooled and hydrated with water via a nozzle system. The laser head of the system hosts the ablation laser and an additional co-axially bundled aiming beam. The low-power continuous-wave Class I green visualization laser allows the surgeon to see the axis of the ablation beam during and also before activating the ablation. The surgeon can only continue with the osteotomy after performing this visual check of the cutting path as a safety-enhancing procedure.

The entire robot-guided laser system is coupled to an intraoperative navigation system. The tracking camera for the navigation system is the fusionTrack 500 (Atracsys®) and mounted on an additional trolley that is an integral part of the CARLO® device. The navigation system is a key safety feature. It monitors the position of the laser with respect to the targeted bone. The system uses two cameras fixed at a known distance and orientation from each other to provide real-time positions of markers fixed to the targeted bone, to the laser head, or to a hand-held pointer used during patient registration. The reference element consists of three or four markers positioned on a rigid object, whose precise position and orientation can be returned by the camera. The accuracy of the navigation system for identifying the position of a single marker depends on the position within the working volume, and it is 0.09 mm to 2 m and 0.15 mm to 2.8 m distance from the camera.

---

## Technical characteristics of CARLO®

---

### Laser source

---

Er:YAG with wavelength $2.94 \mu\text{m}$
Pulse energy 650 mJ
Pulse rate up to 10 Hz
Pulse duration $200 \mu\text{s}$
Power 6.5 W

---

### Robot KUKA® LBR Med

---

Number of axes 7
Max total Payload 7 kg
Accuracy $\pm 0.05 \text{ mm}$

---

## Navigation system

---

Atracsys fusionTrack 500

Pointer Tool NDI, subsequently Pointer tool AOT;  
Art. Nr.: 100094

Laser Head Marker NDI, subsequently Active  
Marker CLH

Target Marker CAsination; subsequently Target  
Marker AOT; Art. Nr.: 100095

---

## 1.5 Motivation for this work

The scientific challenges of this dissertation on cold-ablation and robot-guided laser osteotomies are subdivided as follows:

- To evaluate the clinical usability of this prototype in an operating theatre, the biological safety of the laser had to be checked to prevent potential damage to living tissue. Therefore, we first performed an *in-vivo* study in sheep, in which we assessed the bone healing after use of CARLO<sup>®</sup> and piezosurgery. The healing rate outcomes with the different techniques were compared histologically and with micro-CT analysis.
- To prove in a cadaver study that the laser beam is capable of cutting to a depth of more than 1.5 cm without losing power or inducing carbonization. The evaluation also included an ergonomic analysis and assessment of the applicability of the adopted workflow. Every new step in the development of CARLO<sup>®</sup> was critically reviewed from a clinical and technical perspective.
- To demonstrate the safety, accuracy, and effectiveness of laser osteotomy in a human cadaver lab for various osteotomy patterns and for different cranio-maxillofacial indications including the execution of an interlocking junction between the bone fragments to achieve higher stability. The experiences gained would help the transfer of this technology to a true operating room environment (Figure 2).

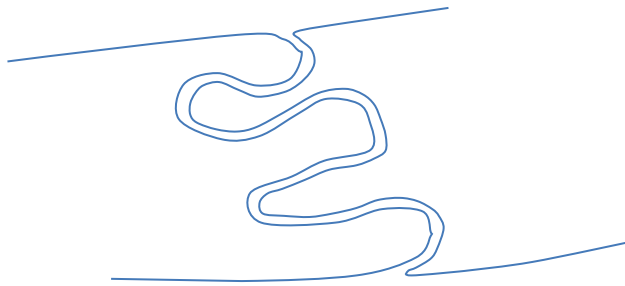


Figure 2: With CARLO®, a macro-retentive pattern could be created on the cutting surface of both bone endings to produce an interlocking junction, which is expected to offer higher stability than straight cuts.

- To get basic knowledge in the biomechanical behavior of different osteotomy patterns.

Coupling the robot-guided laser system to a navigation system, as done in CARLO®, the advantages of performing accurate osteotomies with freely selectable geometries offers new possibilities for patient-specific treatment. To test the different cutting pattern and their impact, incomplete osteotomies on the inner side of the bone flap were simulated with a finite element method. Optimal stress vs. force relation to obtaining the largest projected bone surface will be evaluated. The results may widen the indications for the clinical use of CARLO®, e.g., in weakening bones, which is a major challenge in craniosynostosis surgery to facilitate the re-shaping of the skull (Figure 3).

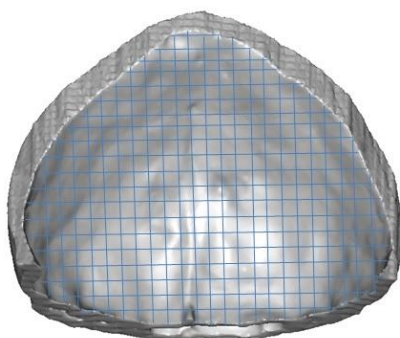


Figure 3: The CARLO® system will be used to generate a pattern of non-perforating osteotomy lines cutting through the inner cortical bone and leaving the outer cortical bone intact. Defining and optimizing the shape and size of the pattern to achieve optimal molding characteristics, while maintaining a reasonable stability is one of the goals of this thesis.

And finally,

- To prepare the use of CARLO® in human clinical trials after approval of the device and the clinical investigation on humans by both Swissmedic (Swiss Regulatory Authority for Medicines and Medical Devices ) and the local ethics committee.

## 1.6 Literature

- 1 Kuttenger JJ, Waibel A, Stübinger S, Werner M, Klasing M, Ivanenko M, Hering P, von Rechenberg B, Sader R, Zeilhofer HF. Bone healing of the sheep tibia shaft after carbon dioxide laser osteotomy: histological results. *Lasers Med Sci.* 2010; 25:239-249
- 2 Krause LS, Cobb CM, Rapley JW, Killoy WJ, Spencer P. Laser irradiation of bone. An in vitro study concerning the effects of the CO<sub>2</sub> laser on oral mucosa and subjacent bone. *J Periodontol* 1997; 68(9):872-880
- 3 Eriksson RA, Adell R. Temperatures during drilling for the placement of implants using the osseointegration technique. *J Oral Maxillofac Surg.* 1986;44(1):4–7
- 4 Eriksson RA, Albrektsson T. Temperature threshold levels for heat-induced bone tissue injury. A vital microscopic study in rabbit. *J Prosthet Dent.* 1983;50(1):101–107
- 5 Augustin G, Zigman T, Davila S, Udilljak T, Staroveski T, Brezak D, et al. Cortical bone drilling and thermal necrosis. *Clin Biomech* 2012;27:313–25
- 6 Field JR, Sumner-Smith G. Bone blood flow response to surgical trauma. *Int J Care Inj* 2002;33:447–51
- 7 Digiovanni CW, Patel A, Calfee R, Nickisch F. Osteonecrosis in the foot. *J Am Acad Orthopaed Surg* 2007;15(4):208–17
- 8 Eriksson RA, Albrektsson T. The effect of heat on bone regeneration using the bone growth chamber. *J Oral Maxillofac Surg* 1984;42:705–11
- 9 Maimann TH, Breinin GM, Schmidt H, Ripps H, Siegel IM, Solon LR. Ocular lesions produced by an optical maser (laser). *Science.* 1961; 134:1525-1526
- 10 Campbell CJ, Noyori KS, Rittler MC, Innis RE, Koester CJ. The application of fiber laser techniques to retinal surgery. *Arch Ophthalmol* 1964; 72:850-857
- 11 Bridges WB. Laser oscillation in singly ionized argon in visible spectrum. *Appl Phys Lett.* 1964; 4:128
- 12 Stern RH, Sognnaes RF. Laser beam effect on dental hard tissue. *J Dent Res.* 1964;43:873
- 13 Pick RM, Colvard MD. Current status of lasers in soft tissue dental surgery. *J Periodontol.* 1993;64(7):589–602
- 14 Tuncer I, Ozçakir-Tomruk C, Sencift K, Cöloğlu S. Comparison of conventional surgery and CO<sub>2</sub> laser on intraoral soft tissue pathologies and evaluation of the collateral thermal damage. *Photomed Laser Surg.* 2010;28(1):75–79
- 15 Horch HH, McCord RC, Keiditsch E. Histological and long term results following laser osteotomy. In: Kaplan I, editor. *Laser Surgery II.* Jerusalem: Academic Press; 1978:318
- 16 Horch HH. Current status of laser osteotomy. *Orthopäde.* 1984;13(2):125–132

- 17 Afilal S. Ablationsmechanismen von biologischem Hartgewebe bei Bestrahlung mit kurzgepulsten CO<sub>2</sub>-Lasern. Doctoral dissertation, Heinrich-Heine-University, Düsseldorf, Germany, 2004
- 18 Parker S. Surgical lasers and hard dental tissue. *Br Dent J* 2007;202: 445–454
- 19 Krause LS, Cobb CM, Rapley JW, Killoy WJ, Spencer P. Laser irradiation of bone. An in vitro study concerning the effects of the CO<sub>2</sub> laser on oral mucosa and subjacent bone. *J Periodontol* 1997;68(9):872-880
- 20 McKee MD. Effects of CO<sub>2</sub> laser irradiation *in vivo* on rat alveolar bone and incisor enamel, dentin, and pulp. *J Dent Res* 1993;72(10):1406-1417
- 21 Peavy GM, Reinisch L, Payne JT, Venugopalan V. Comparison of cortical bone ablations by using infrared laser wavelengths 2.9 to 9.2 micro. *Lasers Surg Med.* 1999;25(5):421–434
- 22 Bader C, Krejci I. Indications and limitations of Er:YAG laser applications in dentistry. *Am J Dent.* 2006;19(3):178–186
- 23 Hibst R. Mechanical effects of erbium:YAG laser bone ablation. *Lasers Surg Med.* 1992;12(2):125–130
- 24 Hibst R, Keller U. Heat effect of pulsed Er:YAG laser radiation. Laser surgery: advanced characterization of therapeutics and systems. *Proc SPIE.* 1990;1200:379–386
- 25 Spencer P, Payne JM, Cobb CM, et al. Effective laser ablation of bone based on the absorption characteristics of water and proteins. *J Periodontol.* 1999;70(1):68–74
- 26 Choi B, Welch AJ. Analysis of thermal relaxation during laser irradiation of tissue *Lasers Surg. Med.* 2001;29:351–359
- 27 Majoran B, Sustercic D, Lukac M, Skaleric U, Funduk N. Heat diffusion and debris screening in Er:YAG laser ablation of hard biological tissues. *Appl Phys B.* 1998;66:1–9
- 28 Gholami A, Baradran-Ghahfarkhi M, Ebrahimi M, Baradran-Ghanfarokhi M: Thermal effects of Laser-osteotomy on Bone: Mathematical Computation Using Maple. *J Med Signals Sens.* 2013;3:262-268
- 29 de Oliveira GJ, Rodrigues CN, Perussi LR, de Souza Rastelli AN, Marcantonio RA, Berbert FL. Effects on Bone Tissue After Osteotomy with Different High-Energy Lasers: An Ex Vivo Study. *Photomed Laser Surg.* 2016;34:291-296
- 30 Stübinger S, Nuss K, Pongratz M, Price J, Sader R, Zeilhofer HF, von Rechenberg B. Comparison of Er:YAG laser and piezoelectric osteotomy: An animal study in sheep. *Lasers Surg Med.* 2010;42:743-751



- 31 Stübinger S, Ghanaati S, Saldamli B, Kirkpatrick CJ, Sader R. Er:YAG laser osteotomy: preliminary clinical and histological results of a new technique for contact-free bone surgery. *Eur Surg Res.* 2009;42(3):150–156
- 32 Sulewski JG. Historical survey of laser dentistry. *Dent Clin North Am.* 2000;44:717–752
- 33 Pourzarandian A, Watanabe H, Aoki A, Ichinose S, Sasaki M, Nitta H, Ishikawa I. Histological and TEM examination of early stages of bone healing after Er:YAG laser irradiation. *Photomed Laser Surg.* 2004;22:342–350
- 34 Sasaki KM, Aoki A, Ichinose S, Yoshino T, Yamada S, Ishikawa I. Scanning electron microscopy and Fourier transformed infrared spectroscopy analysis of bone removal using Er:YAG and CO2 lasers. *J Periodontol.* 2002;73:643–652
- 35 Ivanenko M, Fahimi Weber S, Mitra T, Wierich W, Hering P. Bone tissue ablation with sub-microS pulses of a Q-switch CO2 laser: histological examination of thermal side effects. *Lasers Med Sci.* 2002;17:258–264
- 36 Salina S, Maiorana C, Iezzi G, Colombo A, Fontana F, Piattelli A. A: Histological evaluation, in rabbit tibiae, of osseointegration of mini-implants in sites prepared with Er:YAG laser versus sites prepared with traditional burs. *J Long Term Eff Med Implants.* 2006;16:145–156
- 37 Abu Serriah M, Critchlow H, Whitters CJ, Ayoub A. of partially erupted third molars using an Erbium (Er):YAG Laser: a randomised controlled clinical trial. *Br J Oral Maxillofac Surg.* 2004;42:203–208
- 38 Lee C. A new method to harvest ramus bone using the erbium, chromium:yttrium-scandium-gallium-garnet laser. *J Oral Maxillofac Surg.* 2005;63:879–882
- 39 Dostálová T, Jelínková H, Kucerová H, Krejsa O, Hamal K, Kubelka J, Procházka S. Noncontact Er:YAG laser ablation: clinical evaluation. *Clin Laser Med Surg.* 1998 Oct;16:273-82
- 40 Altshuler GB, Belikov AV, Sinelnik YA. A laser-abrasive method for the cutting of enamel and dentin. *Lasers Surg Med.* 2001;28:435-44
- 41 Ishikawa I, Aoki A, Takasaki AA. Clinical application of erbium:YAG laser in periodontology. *J Int Acad Periodontol.* 2008;10:22-30
- 42 Lubart R, Kesler G, Lavie R, Friedmann H. Er:YAG laser promotes gingival wound repair by photo-dissociating water molecules. *Photomed Laser Surg.* 2005;23:369-72
- 43 Stübinger S, von Rechenberg B, Zeilhofer HF, Sader R, Landes C. Er:YAG laser osteotomy for removal of impacted teeth: clinical comparison of two techniques. *Lasers Surg Med.* 2007;39:583-8
- 44 Rupprecht S, Tangermann K, Kessler P, Neukam FW, Wiltfang J. Er:YAG laser osteotomy directed by sensor controlled systems. *J Craniomaxillofac Surg.* 2003;31:337-42

- 45 Stopp S, Svejdar D, Deppe H, Lueth TC. A new method for optimized laser treatment by laser focus navigation and distance visualization. *Conf Proc IEEE Eng Med Biol Soc.* 2007;1738–1741
- 46 Burgner J, Kahrs LA, Rachzkowsky J, Wörn H: Including parameterization of the discrete ablation process into a planning and simulation environment for robot-assisted laser osteotomy. *Stud Health Technol Inform.* 2009;142:43-8
- 47 Jivraj J, Deorajh R, Lai P, Chen C, Nguyen N, Ramjist J, Yang VXD. Robotic laser osteotomy through prescriptive structured light visual servoing. *Int J Comp Ass Radiol Surg.* 2019;14:809-818
- 48 Brandmeir NJ, Savaliya S, Rohatgi P, Sather M. The comparative accuracy of the ROSA stereotactic robot across a wide range of clinical applications and registration techniques. *J Robotic Surg.* 2018;12:157-163

## **2. Pre-clinical in vivo animal test of craniotomy application in sheep model**

The aim of this preclinical study was to investigate the biology of bone healing after laser irradiation in addition to the applicability in the surgical area. It could be confirmed that bone healing after Er:YAG osteotomy did not impair the healing phase but showed a tendency towards the acceleration of the healing process. In a sheep model, corrective cranial vault surgeries were simulated. The planning workflow was applied: preoperative CT-scanning, virtual planning, registration with the navigation system and navigation controlled and robot-guided laser osteotomy in a series of 12 sheep. Besides the immediately obtained outcome parameters of accuracy of location, shape of the craniotomy, application of the CARLO device, time for the osteotomies, damage of underlying and adjacent tissues, the course of wound healing and the scar formation and new bone were compared to the different osteotomy tools used. The tests were carried out in close cooperation with AOT AG and the VetMedUniversity of Zurich (Prof. B. v. Rechenberg) where the surgeries took place under GLP conditions and approval of the ethical committee and the veterinary office.

Project Leaders: Prof. P. Jürgens / Prof. P. Cattin

Publication: First authorship

---

Augello M, Deibel W, Nuss K, Cattin P, Jürgens P

Comparative microstructural analysis of bone osteotomies after cutting by computer-assisted robot-guided laser osteotome and piezoelectric osteotome: an in vivo animal study.

Lasers in Medical Science

2018 Sep;33(7):1471-1478. doi: 10.1007/s10103-018-2502-0

Impact factor: 1.949

Ranking (H-Index) 58



## Comparative microstructural analysis of bone osteotomies after cutting by computer-assisted robot-guided laser osteotome and piezoelectric osteotome: an in vivo animal study

Marcello Augello<sup>1,2,3</sup> · Waldemar Deibel<sup>4,5</sup> · Katja Nuss<sup>6</sup> · Philippe Cattin<sup>4</sup> · Philipp Jürgens<sup>7</sup>

Received: 9 August 2017 / Accepted: 2 April 2018  
© Springer-Verlag London Ltd., part of Springer Nature 2018

### Abstract

**Objective:** Most industrial laser applications utilize computer and robot assistance, for guidance, safety, repeatability, and precision. In contrast, in medical applications using laser systems are mostly conducted manually. The advantages can be effective only when the system is coupled to a robotic guidance, as operating by hand does not reach the required accuracy.

**Material and Methods:** We currently developed the first laser osteotome which offers preoperative planning based on CT data, robot guidance and a precise execution of the laser cuts. In an animal trial our system was used to create a grid pattern of the same depth on the inner layer of parietal bone in 12 adult sheep

**Results:** The same bone cuts were done with piezoelectric osteotome on the contralateral side. The micro-CT and histological analysis showed more new mineralized bone in the laser group compared to the piezoelectric group. As well a cutting pattern with especially a constant osteotomy depth in the laser group was demonstrated.

**Conclusion:** The here presented autonomous osteotomy tool show not only an advantage in early bone healing stage but additionally sharp bone cuts with a very high accuracy and freely selectable design cuts.

**Keywords:** Laser osteotomy, Er:YAG laser, navigation, bone, nanotome, micro-CT

## Introduction

Currently, conventional mechanical instruments are standard tools in bone surgery. Most of them are conducted manually and used in contact with bone introducing grinding pressure, hammering or similar mechanical forces. Additionally, the cut shape is restricted so that geometrically arbitrary and complex cuts are not achievable [1]. The major advantages of cutting bone with laser light are the freedom in the cutting geometry and the high accuracy. Laser radiation is now used routinely in medical applications to cut, shape, treat, and remove soft tissues of the body. A few publications have reported preliminary success over conventional cutting techniques which include high productivity, narrow kerf width, low roughness of cut surfaces, and minimum distortion [2,3]. Especially the CO<sub>2</sub> laser with a wavelength of 10,6  $\mu\text{m}$  has been associated with a thermal mechanism of bone ablation, with resulting coagulation, vaporization and as a big disadvantage carbonization of living tissues [4]. A breakthrough for cutting and treatment of bone without any histological detectable thermal damage was achieved and investigated by Akyol et al. [5] with the use of an Er:YAG laser. Other studies demonstrated good results in bone healing after Er:YAG osteotomies [6,7]. Nowadays, laser systems and surgical robots in medical field leads to an unergonomic setup due to the big size of the devices. We recently developed the first laser osteotome which offers preoperative planning based on CT data, robot guidance and a precise execution of the laser cuts (figure 1).



**Fig. 1.** The computer-assisted and robot-guided laser osteotome device.

The purpose of this study was to create a grid pattern of the same design on the inner layer of parietal bone in sheep using a piezoelectric (PZE) osteotome as standard tool and to compare bone healing characteristics and the accuracy of the osteotomies by micro-CT and histological observations with the outcomes of the computer-assisted and robot-guided Er:YAG laser osteotome.

## Materials and Methods

### *Computer-assisted and robot-guided laser osteotome system*

For laser osteotomies, an Er:YAG at a wavelength of 2,94  $\mu\text{m}$  was employed (Syneron dental laser, Israel). The laser head is mounted on a light weight robot (KUKA® Light Weight medical grade Robot (LBR iiva), Germany). Furthermore, a green laser was coaxially aligned to the cutting beam, which enables a simulation of the cuts and a real-time position control function for the cutting beam. The tissue being photoablated is permanently cooled and hydrated by a pulsed two twin-fluid nozzle array with external liquid mixture. The laser head is positioned on a KUKA® LBR iiva light-weight robot arm with seven degrees of freedom and integrated sensors for detection of force (KUKA®, Germany). The tracking camera used was the CamBar B2 (Axios 3D®, Germany). The tracking volume accuracy in a distance range of 1.5 – 2.5 m is about 0.14 mm Root-Mean-Square (RMS). All settings were done per our unpublished studies, where we used a fresh ex-vivo sheep skull.

### *Animals and surgical procedure*

A sheep model was used, because sheep have a similar bone metabolism as humans, and thus, results can be directly translated to humans [8-11]. Therefore, twelve swiss alpine sheep at 2-6 years of age, with body weight of 60-90 kg were used in the investigation. Animals were randomly selected and allocated to the treatment groups by hand prior to surgery during the acclimatization phase. All interventions were done in the Musculoskeletal Research Unit of the Vetsuisse Faculty, University of Zurich, Switzerland. The experiments were authorized by the local ethical committee under the license no. 13/2014. Anesthesia consisted of a premedication (0.1 mg/kg BW xylazine, 0.01 mg/kg BW buprenorphine im) and induction (3- 5 mg/kg BW ketamine and diazepam 0.1 mg/kg BW and 1- 4 mg/kg BW Propofol iv). Methadone (0.1 – 0.2 mg/kg BW iv) was given as additional analgesic. Maintenance of anesthetic state occurred via inhalation of isofluran in oxygen with a CRI of propofol (0.1-0.4 mg/kg/min). Utilizing a sterile technique, a biparietal skin incision was executed in the region of the coronal suture to dissect and to retract the coronal flap to expose the fronto-parietal region of the skull. Afterwards quadrangular parietals craniotomies of approximately 2 x 2 cm<sup>2</sup> were pencil marked and paramedially performed to prevent injury to the sagittal sinus. The bone cuts were done with PZE in conventional way to avoid damage to the underlying dura. Then a grid pattern of the same osteotomy depth and design was generated on the inner layer of the skull bone, on the left side with the computer-assisted and robot-guided Er:YAG laser system in a completely autonomous manner. On the right side the same defect was created with the PZE tip OT 7 (Mectron®, Italy, tip thickness 0.55 mm) as control group. For this step the bone flap were fixed to a holding plate with a screw in the middle of the sample from the opposite side; outer layer

of the skull bone (figure 2). The planning of the pattern for the laser group was based on the segmentation of the CT data obtained preoperatively.



**Fig. 2.** A clinical view of a bone probe with the grid pattern performed with the computer-assisted and robot guided laser osteotome. A screw from the opposite side fixed the bone sample during the osteotomy.

The bone probes were then reduced and fixed with resorbable plates and pins (Sonic weld®, KLS Martin, Germany). Wound closure was achieved with resorbable subcutaneous stitches and nylon 3.0 skin sutures. 8 weeks postoperatively, the animals were sacrificed by means of an overdose of sodium pentobarbital injected intravenously. Tissue harvesting was carried out by cutting out the bone samples with the piezo device with a security margin to the osteotomy. The bone pieces were fixated in 40 % Ethanol in individual labeled containers. They were processed per routine until being in 70 % Ethanol.

#### *Micro-CT evaluation*

The amount of the newly formed bone including its mineralization grade and morphology for all 24 bone samples of the biparietal craniotomies (12 laser group, 12 piezoelectric device group) was quantitatively evaluated post mortem with the micro CT scan GE nanotom® m (General Electric, USA) and a modern computer-assisted data processing methods respectively [11]. The three-dimensional data were operated at an acceleration voltage of 60kV and a beam current of 310  $\mu$ A. The 1440 radiographies per data set (exposure time per radiography 2.5 s) were recorded while the bone sample rotated through 360 °. This resulted in a recording time of about four hours per sample. The enlargement was adjusted that the whole sample was set in the view field and resulted in a voxel size of 12  $\mu$ m. For the scan, each sample was positioned in a 50 ml graduated centrifuge tube and embedded in paraffin. Based on these data, the computer reconstructed a 3D image and cut it into slices to produce a 2D image stock. A quantitative 3D histomorphometric evaluation was performed determining the volume of bone mass and of the microarchitecture indices of the newly formed bone on a

cubic volume. The evaluation of the 3D micro-CT data was performed by the 3D volume analysis software Volume Graphics Studio MAX® 2.2 (Volume Graphics GmbH, Heidelberg, Germany) using the scan data to create a three-dimensional model of the volume. An opacity value and a color were assigned to each voxel, depending on its gray value. The bone analysis module within this software was used to measure the bone mineral density within a rectangular region of interest (ROI). The image of the sample was re-oriented in a way that an axial view to the grid pattern of the inner layer of the corticalis was possible. To quantify newly formed mineralized bone and compare it among all samples, a standardized method was used. Five squares of  $3.3 \times 3.3 \text{ mm}^2$  as regions of interest in each sample in the left and right parietal regions were selected in x-y plane of the corners of the samples so that in the center the interjections of the horizontal and vertical osteotomy were located. An equal square was positioned in the center of the bone sample. In the z-plane a  $3 \times 0.8 \text{ mm}^2$  rectangle 1mm below the bone surface was selected as region of interest (ROI) for all 5 chosen areas (figure 3). The x-y plane was centered at the center of the bone sample. Therefore, the ROI number 5, denoted with x-y coordinates equal to (0,0), was at the center of the bone sample.

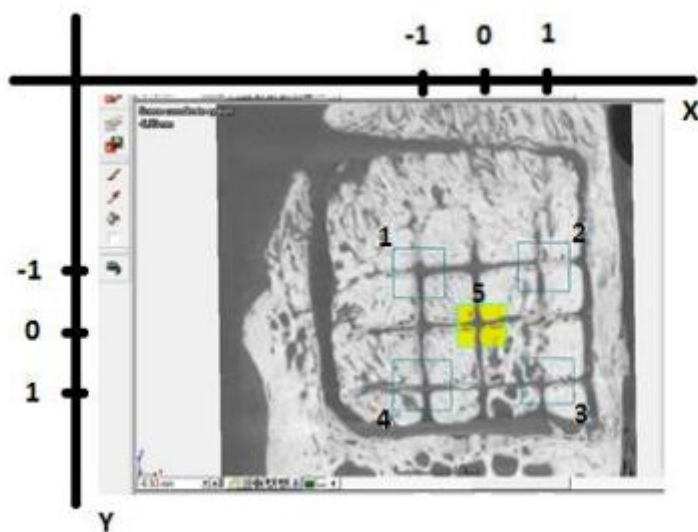


**Fig. 3.** Selected five equally dimensioned cuboids with determination of new bone volume by the threshold function in a cuboid with the software Volume Graphics Studio Max, sample of laser osteotomy, top view.

A total of 10 measurements per sheep were obtained. In such a way 60 samples could be analyzed for the laser group and 60 samples for the PZE group. From the grayscale image a segmented image was created by thresholding. After showing a reasonable binarization of bone structures of a cuboid, by the threshold function total bone and newly formed mineralized



bone was determined. Additionally, the accuracy of a predefined cutting grid was assessed by comparing the symmetry of the mini squares of the grid between laser vs. piezo.

### *Histology*

Sections were cut with a precision saw to slices of 400-750  $\mu\text{m}$  and they were ground to 250-350  $\mu\text{m}$ . Ground sections were surface stained with toluidine blue. Thin sections of 30-100 $\mu\text{m}$  were cut and to visualize the calcium deposits stained with von Kossa/McNeal, Toluidine blue and H&E. The grid was divided into two zones. Zone 1 outer half of the bone towards to the brain and zone 2 towards the skull surface. The evaluated parameters were remodeling activity and stage of bone formation/calcification. Quantitative evaluation of the histology was carried out using computer-based histomorphometric measurements of the sections. These were photographed using a digital camera. Thereafter, the pictures of the perpendicular sections were prepared for measurements by dividing the grid site into 2 sections (left and right) to assess bone resorption and new bone formation individually.

### *Statistics*

The primary endpoint in which the effect of the surgical device was evaluated was the total newly formed bone volume per device per sheep. This measurement was calculated as the sum of the 5 ROI of the left (right) side cranium in each sheep. A paired t-test was used to evaluate the effect of using computer-assisted and robot-guided laser or PZE osteotome on the volume of new bone ( $\text{mm}^3$ ). As well as the difference and 95 % confidence interval of the estimated means were obtained from the paired t-test.

## **Results**

### *Micro-CT findings*

No test item-related mortality was noted. The sheep were sacrificed 8 weeks after surgery according to the protocol. Microstructural analysis using a GE nanotome<sup>®</sup> showed a statistically higher amount of new mineralized bone formation after laser osteotomy compared to PZE osteotomy ( $p < 0.05$ ). A representative view is shown in figures 4a and 4b. Top views of the specimen demonstrated a more accurate and symmetrical osteotomy of the grid pattern in the laser group.

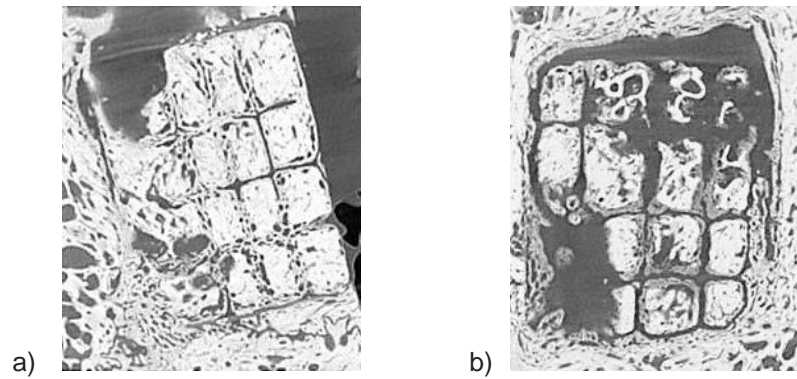


**Fig. 4a and b:** Top view of osteotomy examples after laser (a) and PZE osteotomy (b).

Additionally, the lateral view revealed a constant depth of the osteotomies in the laser group while the cutting depth in the PZE group varied greatly. The mean (SD) total new mineralized bone volume was 26.2 mm<sup>3</sup> (6.5) for laser and 24.4 mm<sup>3</sup> (11.95) for PZE osteotomy, although the original bone volume was higher in the PZE group; 32.7 mm<sup>3</sup> (11.21) for laser vs. 42 mm<sup>3</sup> (17.19) for PZE (table 1). Therefore, the percentage of new bone volume resulted higher after laser osteotomy compared to PZE osteotomy (45.61 % vs. 37.78 %). The results demonstrated a 95% CI equal to [-5.3, 8.9] and a  $p < 0.05$ . When considering all ROI measurements in a linear mixed model to evaluate overall differences between surgical procedures, the estimated mean difference and 95 % was equal to [-0.3, 1.2]. The linear mixed model had the added advantage of including all locations of the ROIs in the model to check whether location had any impact on measuring the effect of the surgical procedures. Table 1 depicts the individual values of the percent of new bone volume for each sheep's osteotomy using laser and piezo devices. The results represent the mean values for laser and PZE devices. Each line connects the individual new bone values for each of the 12 sheep. Note that the new bone values obtained from the laser group are higher in all sheep probes except in sheep 3 which reached the same value of the PZE. The top view of the bone probes additionally confirmed that the pattern in the laser group was more exact and symmetrical.

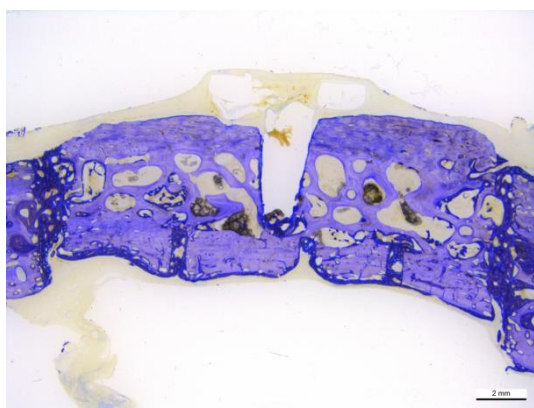
**Table 1.** New mineralized bone in 12 sheep after 8 weeks expressed in volume and percent of the original bone amount.

New bone (mm <sup>3</sup> )	Statistics	Laser	PZE
<b>Total</b>	n	12	12
	mean (SD)	26.2 (6.5)	24.4 (11.95)
	median (Q1,Q3)	25.3 (22.96, 30.66)	23.1 (13.18, 35.61)
	min-max	12.9 – 36.9	10.1 – 46.9
<b>ROI location</b>			
I	n	12	12
	mean (SD)	5.5 (1.97)	4.7 (2.51)
	median (Q1,Q3)	6.4 (4.21, 7.16)	3.9 (2.74, 6.95)

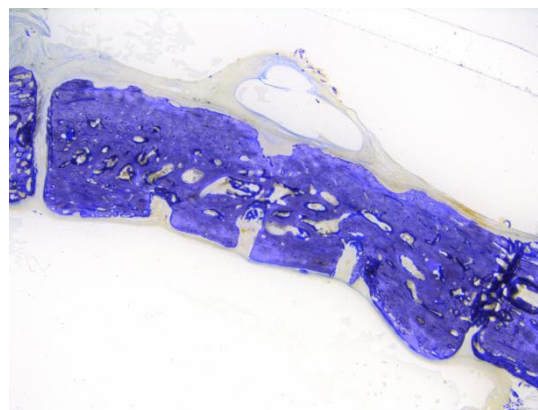
	min-max	2 – 7.5	1.6 – 8.9
2	n	12	12
	mean (SD)	5 (1.72)	5.2 (3.49)
	median (Q1,Q3)	4.5 (3.8, 6.29)	4 (2.69, 7.27)
	min-max	2.7 – 8.1	1.6 – 13.6
3	n	12	12
	mean (SD)	5.1 (1.96)	4.3 (2.42)
	median (Q1,Q3)	4.5 (3.67, 6.82)	3.6 (2.37, 5.53)
	min-max	1.9 – 8	1.6 – 9.2
4	n	12	12
	mean (SD)	5 (1.51)	5.4 (3.41)
	median (Q1,Q3)	5.1 (3.98, 6.03)	5.1 (3.04, 6.66)
	min-max	1.9 -7.2	1.2 – 14
5	n	12	12
	mean (SD)	5.7 (1.39)	4.9 (2.64)
	median (Q1,Q3)	5.3 (4.38, 7.1)	4.2 (2.67, 6.82)
	min-max	4.2 – 7.6	1.8 – 9.4
<b>Percent of new bone (%)</b>	<b>Statistics</b>	<b>Laser</b>	<b>PZE</b>
<b>Total</b>	n	12	12
	mean (SD)	45.61 (11.7)	37.78 (7.21)
	median (Q1,Q3)	42.7 (39.33, 49.91)	37.9 (32.21,41.47)
	min-max	31.2 - 70.6	23.5 - 49.1
<b>ROI location</b>			
1	n	12	12
	mean (SD)	44.6 (11.29)	35.8 (9.67)
	median (Q1,Q3)	41.5 (36.09,50.17)	34.7 831.92, 42.73)
	min-max	30.7 - 71.3	15.3 - 52.6
2	n	12	12
	mean (SD)	44.5 (13.53)	35.9 (11.48)
	median (Q1,Q3)	40.1(36.02, 48.5)	36.8 (29.14, 43.59)
	min-max	28.1- 78.9	19 - 65.2
3	n	12	12
	mean (SD)	49.9 (10.82)	42.4 (9.98)
	median (Q1,Q3)	48.7 (39.45, 62.6)	32.7 (26.94, 36.95)
	min-max	23 - 78.9	19 - 65.2
4	n	12	12
	mean (SD)	44.5 (10.82)	38.5 (9.98)
	median (Q1,Q3)	42.4 (37.1, 52.63)	43.6 (38.46, 47.769)
	min-max	29.1 - 62.6	23.6- 60.2
5	n	12	12
	mean (SD)	44.4 (14.98)	36.3 (8.52)
	median (Q1,Q3)	39.7 (32.45, 54.16)	35 (29.5, 41.83)
	min-max	28.5 - 74.6	25.08 - 51

### *Histological findings*

The osteotomies of the grids showed less fibrous tissue where laser was used for bone cutting in comparison to PZE. Values for new bone were higher for the grids in the laser group so that between the osteotomy areas a thicker layer of newly formed bone could be demonstrated (figures 5a and b). The examination of the present immune cells showed no pronounced inflammatory or degradative reaction in both groups.



a)



b)

**Fig. 5a and b:** Side view of osteotomy and grid pattern of histological sections, a) computer-assisted and robot-guided Er:YAG laser osteotome and b) PZE, (C = craniotomy).

## Discussion

In this *in vivo* study, we compared osteotomies of the inner layer of parietal bone in a sheep model done by a computer-assisted and robot-guided Er:YAG laser and a PZE device in terms of precision of the cuts and new bone formation by micro-CT and histology. While bone healing of many animal species is recognized to be faster than in humans, sheep are considered to have a bone healing rate similar to humans and have been previously established as useful models for human bone turnover and remodeling activity [12,13]. The computer-assisted and robot-guided Er:YAG laser osteotome can be characterized as an innovative, non-contact, vibration-free surgical method with the prevention of massive bone mill and metal abrasion and with supplementary freely selectable choice of cut geometry. The clinical applicability of this device was already described by Baek et al. [14]. In contrast, PZE osteotomy turned out to be an advanced, ultrasound-based technique with direct contact between the bone surface and the cutting tips. Previous studies have shown that the Er:YAG laser with a wavelength of 2.94  $\mu\text{m}$  has a strong absorption coefficient for water. In addition, the organic matrix and inorganic calcium salts, the major component found in bone, also have a very high absorption coefficient for Er:YAG laser irradiation [15-17]. Because of this high absorption, the mechanism of bone ablation is thermally mediated by explosive pyrolysis of the substrate. This means, if the required energy is delivered into the target within a very short time and at a high instantaneous power, then the energy has little time to escape from the ablated volume, and consequently minimal heat is diffused into the surrounding tissue. Control of the extent of lateral damage during laser irradiation is based primarily on the speed of the laser application, the faster the pulse, the less the time available for conduction into adjacent tissue [18]. In this work neither

carbonization nor inflammatory nor necrosis signs have been shown. Similar findings were reported in other studies [19,20]. Although the principles of the bone ablation process of contact free laser osteotomy and contact PZE osteotomy are completely different, the direct comparison of bone healing in our in vivo study revealed in the measurements of the micro-CT data a statistical significance in the laser group. As well the histological outcomes showed a clearly higher volume of new bone formation. Similar results with a higher tendency of new bone formation were confirmed by Gabric et al. [21]. The main endpoint, the overall new bone volume per bone probe (surgical device) per sheep, had the advantage of providing information from different locations in which the osteotomy was performed. If we consider the absolute values of the new bone formation, then we will reach higher values in the laser group compared to the PZE group. And if we also assume that the percent of new bone formation as indicative for bone regeneration, then the differences show statistic significant higher amount of new bone formation after Er:YAG laser osteotomies. Moreover, when the individual ROIs in microstructural analysis were examined, the same conclusions for surgery procedures were obtained. A possible explanation for these differences could be in the anatomy of the bony structure captured for micro-CT scans (ROIs). If more cortical parts were detected, a larger bone surface was present for the bone formation. This active surface was in the case of an imaging of a more spongiform surface smaller, resulting in less bone formation. Therefore, we are convinced that the results of the osteotomies with the Er:YAG laser have a stronger new bone formation compared to the PZE group. One possible explanation for these findings shows scanning electronic microscope observations [22]. The osteotomy with laser leaves a same pored bone surface as untreated bone because of thermomechanical ablation. By contrast, in the osteotomy with PZE, the resulting bone mill is pressed into the bone. This bone mill must be removed by the bone cells in the early bone healing phase which leads to a delay in the healing process.

With the here presented computer-assisted and robot-guided Er:YAG laser osteotome complex and arbitrary cutting geometries are feasible. The microstructural analysis with a micro-CT, which allows an exact 3D evaluation of the structures, showed symmetric cutting pattern. Thus, with the proposed computer-assisted and robot-guided Er:YAG laser osteotome, working in a completely autonomous way, cutting accuracies are obtainable which are unachievable by manual laser application. The osteotomies performed with the laser in our study are more time consuming compared to PZE depending on the bone thickness. Nevertheless, the system opens up new perspectives showing more advantages, e.g. less bone loss, precise execution, improved and faster healing with reducing the patient's morbidity. In case of bone reconstruction with a bone flap the realization of a predefined bone cut such as swallowtails as macro-retentive patterns, achieve an optimum fit of the bone edges to each other producing an interlocking junction and consequently a higher stability than straight cuts

can be provided. Therefore, a less rigid plate system for osteosynthesis would be necessary. Further investigations in biomechanics are here needed. Another use of the presented system could be the corrective surgery of craniosynostosis. The surgical steps consist in perform the craniotomy with special preoperatively calculated cutting geometries and additionally to perform incomplete osteotomies on the inner side of the bone flap to facilitate the re-shaping (skull moulding). This complex surgical pathway could be significantly shortened with less blood loss. To preserve underlying vital structures, e.g. blood vessels, nerves, dura mater, the state of the art is a video camera-based control of laser ablation as proposed by Kahrs et al. [23]. However, more accurate and reliable detection of the remaining bone to cut could be achieved by applying optical coherence tomography (OCT) as online sensing technique [24].

## **Conclusion**

With the here presented computer-assisted and robot-guided Er:YAG laser osteotome a statistically higher new bone formation compared to PZE osteotomy has been reached. The results were confirmed by micro-CT scans and histological analysis. Additionally, a symmetric cutting pattern with especially a constant osteotomy in depth has been shown in the test device group. Further studies with human cadavers are to be carried out to validate the system before clinical use.

## **Acknowledgments**

We gratefully acknowledge Dr. Georg Schulz, Biomaterials Science Center, University of Basel, Switzerland, for performing the micro-CT scans.

## References

- [1] Burgner J, Muller M, Raczkowsky J, Worn H. (2010) Ex vivo accuracy evaluation for robot assisted laser bone ablation. *Int J Med Robot.* 6:489–500
- [2] Stübinger S, Ghanaati S, Saldamli B, Kirkpatrick CJ, Sader R. (2009) Er: YAG laser osteotomy: preliminary clinical and histological results of a new technique for contact-free bone surgery. *Eur Surg Res.* 42:150–156
- [3] Kuttenger JJ, Stübinger S, Waibel A, Werner M, Klasing M, Ivanenko M, Hering P, Von Rechenberg B, Sader R, Zeilhofer HF. (2008) Computer-guided CO<sub>2</sub>-laser osteotomy of the sheep tibia: technical prerequisites and first results. *Photomed Laser Surg.* 26:129-136
- [4] Kuttenger JJ, Waibel A, Stübinger S, Werner M, Klasing M, Ivanenko M, Hering P, von Rechenberg B, Sader R, Zeilhofer HF. Bone healing of the sheep tibia shaft after carbon dioxide laser osteotomy: histological results (2010) *Lasers Med Sci.* 25:239-249
- [5] Akyol UK, Güngörmüş M, Gündoğdu C, Erdem H. (2009) Histologic evaluation of the effects of Er: YAG laser on bone ablation. *J Contemp Dent Pract.* 10:65–72
- [6] Kesler G, Romanos G, Koren R. (2006) Use of Er:YAG laser to improve osseointegration of titanium alloy implants – a comparison of bone healing. *Int J Oral Maxillofac Implants.* 21(3):375-379
- [7] Stübinger S, Biermeier K, Bächli B, Ferguson SJ, Sader R, von Rechenberg B. (2010) Comparison of Er:YAG laser, piezoelectric, and drill osteotomy for dental implant site preparation: biomechanical and histological analysis in sheep. *Lasers Surg Med.* 42(7):652-661
- [8] Nunamaker D. (1989) Experimental models of fracture repair. *J Clin Orthop Rel Res.* 5:355
- [9] Augat P. (1998) Local tissue properties in bone healing: Influence of size and stability of the osteotomy gap. *J Orthopaed Res.* 16:475–481
- [10] Sarkar M, Patka P, Kinzl L. (2001) First histological observations on the incorporation of a novel calcium phosphate bone substitute material in human cancellous bone. *J Biomed Mat Res.* 13:329–334
- [11] Schulz G, Götz C, Müller-Gerbl M, Zanette I, Zdora MC, Khimchenko A, Deyhle H, Thalmann P, Müller B. (2016) Multimodal imaging of the human knee down to the cellular level. *X-Ray Microscopy Conference: J Physics.* 849:1-4
- [12] Martini L, Fini M, Giavaresi G, Giardino R. (2001) Sheep model in orthopedic research: a literature review. *Comp Med.* 51:292-299.
- [13] Fagundes DJ, Taha MO. (2004) Modelo animal de doença: critérios de escolha e espécies de animais de uso corrente. *Acta Cir Bras.* 19:59-65

- [14] Baek KW, Deibel W, Marinov D, Griessen M, Dard M, Bruno A, Zeilhofer HF, Cattin P, Jürgens P. (2015) Clinical applicability of robot-guided contact free laser osteotomy in cranio-maxillo-facial surgery: in-vitro simulation and in-vivo surgery in minipig mandibles. *Br J Oral Maxillofac Surg.* 53:976-981
- [15] Bayly JG, Kartha VB, Stevens WH. (1963) The absorption spectra of liquid phase H<sub>2</sub>O, HDO, D<sub>2</sub>O from 0.7µm to 10 µm. *Infrared Phys.* 3:211-223
- [16] Doyle BB, Bendit EG, Blout ER. (1975) Infrared spectroscopy of collagen and collagen-like polypeptides. *Biopolymers.* 14:937-957
- [17] Miller GL. (1952) Improved infrared photography for electrophoresis. *Science.* 116:687-688
- [19] Trost D, Zacherl A, Smith M. (1992) Surgical laser properties and their tissue interaction. St. Louis: Mosby-Year Book
- [19] Sasaki KM, Aoki A, Ichinose S, Yoshino T, Yamada S, Ishikawa I. (2002) Scanning electron microscopy and Fourier transformed infrared spectroscopy analysis of bone removal using Er:YAG and CO<sub>2</sub> lasers. *J Periodontol.* 73:643-652
- [20] de Oliveira GJ, Rodrigues CN, Perussi LR, de Souza Rastelli AN, Marcantonio RA, Berbert FL. (2016) Effects on bone tissue after osteotomy with different high-energy lasers: an ex vivo study. *Photomed Laser Surg.* 34:291-296
- [21] Gabric D, Blaskovic M, Gjorgijevska E Mladenov M, Tasic B, Juric IB, Ban T. (2016) Evaluation of bone healing after osteotomies prepared with Er:YAG laser in contact and noncontact modes and piezosurgery-an animal study. *J Oral Maxillofac Surg.* 74:18-28
- [22] Baek KW, Deibel W, Marinov D, Griessen M, Dard M, Bruno A, Zeilhofer HF, Cattin P, Jürgens P. (2015) A comparative investigation of bone surface after cutting with mechanical tools and Er:YAG laser. *Lasers Surg Med.* 47:426-432
- [23] Kahrs LA, Burgner J, Klenzner T, Raczowsky J, Schipper J, Wörn H. (2010) Planning and simulation of microsurgical laser bone ablation. *Int J Comput Assist Radiol Surg.* 5:155-162
- [24] Zhang Y, Pfeiffer T, Weller M, Wieser W, Huber R, Raczowsky J, Schipper J, Wörn H, Klenzner T. (2014) Optical coherence tomography guided laser cochleostomy: towards the accuracy on tens of micrometer scale. *Biomed Res Int.* 11:251-284



### 3. Wet lab human fibulae osteotomies

After the promising results of the first study that bone healing after laser osteotomy was even associated with faster bone healing than with piezo osteotome, the next investigation followed in the lab.

Firstly, we had to examine whether the performance of our laser source to cut larger bone thicknesses. Experience has shown that a fibula is approximately 1.2 to 1.8 cm wide. For this purpose, tests were done with two human male fibulae from the Anatomical Institute of the University Basel. These fibulae were preserved in formaldehyde. The maximum thickness was 1.6 cm. Secondly, a conclusive workflow for using CARLO® for mandibular reconstruction with fibula free flap was established and evaluated. Starting with a straight cut, we could see that the laser beam achieved to remove the bone layer by layer effortlessly. In the end, we had a clean-cut surface without signs for carbonization. Very motivated followed more cuts, these with a swallowtail like cut (see figures below). Confirming the capability of the Er:YAG performance with our parameters to cut at least a depth of 1.6 cm in this dummy test. The next step was to go into a cadaver study.



Figure 3.1: Setup wet lab: The fibulae were fixed on the tracking plate with adhesive tape. The bone cut was done by ad hoc planning.



Figure 3.2: Cutted fibulae. In the upper position a cutted fibula with straight pattern and a thickness of 1.6 cm. In the lower position the second fibula with swallowtail like bone incision geometry.

#### **4. Workflow for using CARLO® for mandibular reconstruction with fibula free flap and midfacial osteotomies**

Confirming the system's performance in the dummy tests, the applicability of the workflow had to be verified in an operating room environment. Therefore, based on CT scans of upper, lower jaw and fibulae of six human cadavers' 3D virtual plans were executed to perform partial mandibulectomy and reconstruction with fibula free flap. The cutting edges of the wedges to fold the fibula were modified with "smart" cuts: a macro-retentive pattern was created on the cutting surface of both bone endings to produce an interlocking junction. Additionally, mandible splits and Le Fort I osteotomies were done. The evaluation included an ergonomics analysis about the position of the CARLO device in relation to the patient and the development of easy to use instruments to attach navigational markers to the fibula bone and perform the referencing of the whole system. Also, the duration of the bone cuts were registered.

Project Leaders: Prof. P. Jürgens / Prof. P. Cattin

Publication: First authorship

---

Augello M, Baetscher C, Segesser M, Zeilhofer HF, Cattin P, Juergens P.

Performing partial mandibular resection, fibula free flap reconstruction and midfacial osteotomies with a cold ablation and robot-guided Er:YAG laser osteotome (CARLO®) - A study on applicability and effectiveness in human cadavers.

J Craniomaxillofac Surg. 2018 Oct;46(10):1850-1855.

doi: 10.1016/j.jcms.2018.08.001.

Impact factor: 1.960

Ranking 10/46 (H-Index) 64

---



## Performing partial mandibular resection, fibula free flap reconstruction and midfacial osteotomies with a cold ablation and robot-guided Er:YAG laser osteotome (CARLO®) – A study on applicability and effectiveness in human cadavers



Marcello Augello <sup>a, b, \*</sup>, Cyrill Baetscher <sup>c</sup>, Mireille Segesser <sup>c</sup>, Hans-Florian Zeilhofer <sup>b, d</sup>, Philippe Cattin <sup>e, 1</sup>, Philipp Juergens <sup>b, d, 1</sup>

<sup>a</sup> Department of Cranio-Maxillofacial Surgery, (Head: Prof. Dr. Dr. Dr. H.C. Hans-Florian Zeilhofer), Hospital Aarau, Aarau, Switzerland

<sup>b</sup> Hightech Research Centre of Cranio-Maxillofacial Surgery, University of Basel, Allschwil, Switzerland

<sup>c</sup> Advanced Osteotomy Tools AG, Basel, Switzerland

<sup>d</sup> Department of Cranio-Maxillofacial Surgery, University Hospital, Basel, Switzerland

<sup>e</sup> Center for Medical Image Analysis and Navigation, University of Basel, Allschwil, Switzerland

### Abstract

**Objective:** Aim of the study was to prove the safety, accuracy characteristics of contact-free laser osteotomy executed with the cold ablation and robot-guided Er:YAG laser osteotome in a human cadaver test.

**Material and Methods:** On six human cadavers mandible resections with a swallowtail like pattern were performed with the laser system on each side. The defects were reconstructed with a fibula graft of identical design and enlarged by 0.2 units. Mandibles and fibulas width as well surgery times were recorded. Additionally a Le Fort I and median mandible split were done. Macroscopically, the bone margins were examined for necrosis.

**Results:** Laser osteotomies of the mandible up to a depth of 23 mm were possible without any thermal damage. Repeatability and precision of the system could be easily assessed. With the navigation system precise control of localization was achievable. Mean surgery time for the mandible resection was 13.32 minutes and for the fibula osteotomy 12.38 minutes.

**Conclusion:** The simply transmission of a cold ablation and robot-guided laser osteotome in an operation room identical environment for surgical interventions could be demonstrated. Precise osteotomy patterns with freedom in the design and carbonisation-free cut surfaces have been shown.

## Introduction

Surgical interventions in the viscerocranium require maximum precision to achieve optimal functional and aesthetic results. Publications show, that there is still room for improvement when applying conventional procedures (Zaret et al. 1961, Taylor et al. 1965.). Thus, there is still a strong clinical need to provide techniques which can achieve higher accuracy. State-of-the-art osteotomy techniques use mechanical rotating, oscillating or piezo surgery tools. The large variety of different tools for drilling and cutting have in common, that they only provide very limited freedom in their cutting geometries (straight or gently curved lines and holes). These cut-faces typically lead to a load-bearing osteosynthesis. Additionally, the interaction between tool and hard tissue can cause mechanical and thermal damage leading to necrosis of the bone tissue at the cutting faces (Stuebinger et al. 2010, Stuebinger et al. 2007). The creation of new –functional – cutting geometries, providing an interconnective cut-face would allow a primarily stable load-sharing connection between the bone segments. A solution to achieve functional cuts could be, to perform the osteotomies with an Erbium-doped yttrium aluminum (Er:YAG) lasers emitting in the infrared spectrum with a wavelength of 2.94  $\mu\text{m}$ . In a retrospective clinical study, an Er:YAG laser used for minor osteotomy in oral and maxillofacial surgery, the laser revealed a remarkable cutting efficiency without any visible (thermal) side effects (Meijer 2004, Stuebinger et al. 2009). Er:YAG lasers emit at a wavelength corresponding to one strong absorption peak of water (3  $\mu\text{m}$ ). This leads to an ablating of tissue. As the laser is ablating the tissue, and not cutting the bone at once, as conventional instruments do, a robot assisted surgery system is necessary in combination of this new cutting technique. Most industrial laser applications utilize robot assistance (Afzal 2004). In contrast, lasers in medical applications are mostly controlled by hand nowadays. However, industrial laser applications cannot just be transferred into clinical and surgical use. The patient, as an inaccurately defined workpiece, with its individual anatomy and pathology, ultimately needs a “single lot” planning. We currently experimenting with the first cold ablation robot-guided laser osteotome (CARLO®) which offers preoperative planning with functional laser cut geometries and a navigation system for a precise execution. Due to the complex three-dimensionality of the anatomy and the proximity of vulnerable structures in the head, the field of cranio-maxillofacial surgery is ideal to demonstrate the advantages of this new osteotome. In our preclinical study, we exemplarily illustrate the use of CARLO® for osteotomies in the midface and osteotomies and reconstructions in the mandible. We performed free fibula flap reconstructions with a swallow tail cut, mandibula splits and le Fort I osteotomies with sinusoidal cuts. The accuracy of the executed plan and the stability of the mandible reconstruction must be tested for clinical applicability and effectiveness. This is, to our knowledge, the first human cadaver trial of this kind, aiming to demonstrate the safety,

accuracy and effectiveness of a contact-free laser osteotomy executed with a robot-guided Er:YAG laser device. It is expected that the experiences gained in this close-to-real setup can be seamlessly transferred into a true operating room environment.

## Materials and Methods

The cadaver tests were conducted on six Thiel fixated cadavers irrespective of gender, age or race. A corresponding approval from the local ethics committee was available (EKNZ 2014-352). Intact maxillae, mandibulae and fibulae were required. In each cadaver, a defect of 4cm in the body of the mandible, with functional swallowtail like cuts at the proximal and distal end of the defect site, has been osteotomized (figure 1).



**Figure 1:** View on the right partially toothed mandible after laser osteotomy of a 4 cm defect with functional cuts. No carbonization has been seen.

Afterwards the defect of the mandible was reconstructed with a fibula free flap from the right lower extremity. The corresponding bone piece was intended to produce an interlocking press fit. Le Fort I osteotomies and median mandible splits were additionally executed to demonstrate the applicability and the effectiveness of the system for a variety of indications in the field of CMF surgery to be treated with the CARLO<sup>®</sup> system.

*Cold ablation robot-guided Er:YAG laser osteotome system CARLO<sup>®</sup>*

For laser osteotomies, an Er:YAG laser with a wavelength of 2,94  $\mu\text{m}$  was employed. It is a custom-made miniaturized laser system developed by the swiss start-up company Advanced Osteotomy Tools in Basel (AOT, Switzerland). The class IV Er:YAG ablation laser is held and guided by a tactile robot (KUKA<sup>®</sup> Light Weight medical grade Robot (LBR MED), Germany) which is controlled by a navigation system. The laser head of the system hosts the ablation laser and, additionally, a visualization laser for enhanced safety which is co-axially bundled. The low-power continuous-wave Class I green visualization laser indicates the osteotomy path at all times. The visualization laser is not only used during the ablation process to make the invisible (infrared) class IV cutting laser beam visible, but also to confirm the potential osteotomy path prior cutting. Before the osteotomy is started, the process foresees a dry run with the visualization laser to indicate the osteotomy path to be. Only once the surgeon confirms the potential cutting path, the ablating system will start. The FusionTrack 500 tracking camera (Atracsys<sup>®</sup>, Switzerland) for the navigation system is mounted on an additional trolley and is an integral part of the CARLO<sup>®</sup> device. The tracking volume accuracy at a distance range of 1.5 – 2.5 m reached about 0.14 mm Root-Mean-Square (RMS). Saline solution and medical air was used for the nozzle system to create the cooling spray. All CARLO<sup>®</sup> settings were done according to our unpublished studies, where we used fresh ex-vivo sheep skulls. Matching the preoperative planning to the anatomy was done by fixing patient markers to the anatomical region in question and then pointing at preoperatively predefined landmarks with a pointer tool. Both patient marker and pointer tool carry reflectors which can be traced in space by the navigation system.

### *Surgical technique*

Before the surgery started, the cold ablation robot-guided laser osteotome along with its tracking camera trolley was placed (on the cadaver left side) so that the intervention could be done without obstructing the work of the surgeon on patient right side. For the partial mandible reconstruction with a fibula free graft indication both operation sites, i.e. the mandible and the fibula were easily accessible. Access to the right corpus mandibulae was gained by a standard neck procedure. The marker device for intraoperative navigation was fixed to the paramedian area of the left mandible so that it was not interfering with the movement of the robot arm during the intervention. In dentate specimen, a temporary intermaxillary fixation using 3 IMF screws in each jaw and 0.5 mm wire loops was applied. Subsequently, the functional cut (i.e. swallow tail cut) in the corpus mandibulae was virtually planned distally to the mental foramen. The planning was then projected onto the lower jaw by the visualization laser so that the surgeon was able to check the prospective osteotomy in situs. To protect the underlying tissue from being cut, a retractor was positioned beneath the mandible. Once the osteotomy in the

mandibula was completed the set-up had to be changed to perform the osteotomy on the lower right extremity. Lateral access to the fibula was gained with its exposition from the caput fibulae to the lateral malleolus. The patient marker was fixed to the proximal part of the fibula. The same swallowtail osteotomy pattern as in the mandible with an offset of 0.6 units to compensate for the cutting with was placed and visualized onto the exposed fibula and confirmed by the surgeon. After harvesting the fibula graft, it was locked by press fit into the lower jaw defect (figure 2).



**Figure 2:** Defect reconstruction with a free fibula bone graft with the same swallowtail shaped cut pattern as for the mandible osteotomy in press fit technique.

The CARLO® device was also used for Le Fort I osteotomies. Access to the maxilla was gained with a routine incision into the healthy cuff of sliding gingiva. As osteotomy pattern a sinusoidal cut was chosen with a wave length of 5mm (figure 3a). After the cut and the subsequent down fracturing of the maxilla, the position of the fragment could be passively adjusted to a more anterior or posterior position. The shifting depended on the wave length of the functional sinusoidal osteotomy (in our case every 5 mm) (figure 3b).





a)



b)

**Figures 3a and b:** Sinusoidal osteotomy in Le Fort I level bilaterally (a). After down fracture of the maxilla the bone piece can be easily repositioned offset according to the width of the osteotomy pattern (b). In this case a posterior positioning is showed (pencil marked).

For the median mandible split, similar to the Le Fort I osteotomy, a sinusoidal wave cut was selected. The length of the sinus amplitude was 8mm (figure 4). Again, to protect the underlying tissue from being cut, a retractor was positioned beneath the mandible.



**Figure 4:** Mandible split with a sinusoidal osteotomy pattern

The osteotomy was successfully performed in an equal manner as described in the above indications. In all cuts, no sign of charring or overheating of any kind could be found (Figure 5).



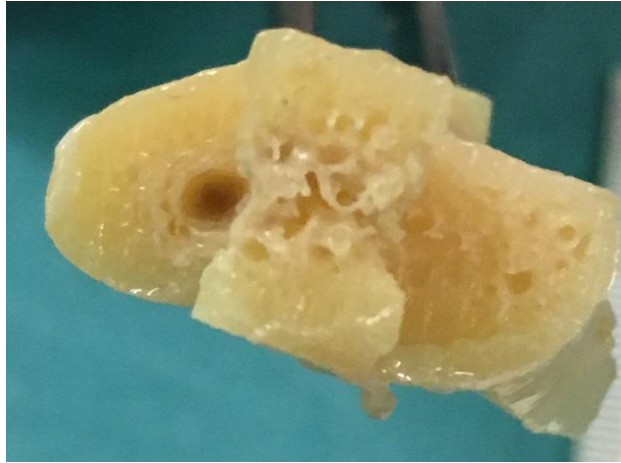


**Figure 5:** Top view on an osteotomized surface after mandible resection with no carbonization signs.

## Results

The tests were conducted on three male and three female corpses in a near identical operation theatre environment without substantial alteration to the position of the specimens. The test device carried out the osteotomies by shifting its position from the head to the lower extremities. The surgeon was able to perform all interventions without any disturbances from CARLO<sup>®</sup>. Likewise, the tissue retractors constituted no obstacle for the laser device during the osteotomies. No safety issues occurred. The execution of the preoperatively planned and intraoperatively navigated osteotomies could be carried out successfully. In the three male corpses, the planned 4cm resection width could be respected. In cases with female specimens, the resection width was not possible. The posterior part of the osteotomy line was too far back, so that the cut interfered with ramus ascendens of the mandible. In the female specimens, the average resection width was 3.2 cm. The maximum of bone breadth of the mandible was up to 2.3 cm (mean 1.9 cm) and for the fibula 2.1 cm (mean 1.7 cm, table 1). Measured mean surgery time for the mandible resection was 13.3 minutes and for the fibula osteotomy 12.3 minutes. The bone specimens could be cut efficiently with a cutting width of 0.5 mm. A cutting off set of 0.6 units to compensate for the cutting width of the laser and to achieve an interlocking swallowtail press fit for the reconstruction of the mandible with the fibula flap graft was chosen. The functional cuts resulted in a reconstructed situation with higher primary stability than done with straight cuts. Depending on the preoperatively determined width of the sinusoidal cutting pattern for the Le Fort I osteotomy, an exact posterior or anterior offset positioning of the

maxilla could easily be achieved. For the mandibula split, the functional cuts resulted in a reconstructed situation with higher primary stability than done with straight cuts, additionally the reconstruction was very easy to achieve. The cutting width in all cases was 0.5mm. No thermal damage in terms of carbonization was macroscopically seen in any of the osteotomized bone fragments and the cut face remains open porous (i.e. the harversian canal intact - figure 5). No injuries to the underlaying soft tissues of the osteotomies were observed.

**Table 1**  
Gender characteristics and values of mandible and fibula widths with duration of the osteotomies.

Specimen		Mandible width (cm)		Surgery time (min)		Fibula width (cm)		Surgery time (min)	
		Right	Left	Right	Left	Prox	Dist	Prox	Dist
1	male	2.3	2.2	17.67	17.55	1.6	1.5	15.5	14.17
2	male	1.9	1.8	15.07	14.93	1.4	1.3	14.73	13.25
3	female	1.6	1.6	12.5	12.93	1.3	1.4	12.28	12.66
4	female	1.4	1.5	9.58	10.05	1.3	1.1	11.5	9.64
5	male	1.8	1.9	13.22	12.8	1.4	1.3	13.11	12.74
6	female	1.7	1.6	10.08	10.25	1.1	1.2	8.93	10.15
	mean	1.78		13.32		1.33		12.38	

## Discussion

A literature research in Pubmed and Cochrane Library showed that to date very little data has been published regarding robot-assisted laser systems. First tests with a robot assisted laser system for bone ablation were done by Burgner et al. (2010) using fresh ex vivo half-skulls from pigs. Predefined cutting patterns were performed on mandibles with a short-pulsed CO<sub>2</sub> laser. The evaluation of the accuracy has shown the applicability of such devices. To our knowledge, no autonomous, contact free osteotomy devices are available in the medical field today. Industrial laser applications are used for high volume products. The thermal load of these lasers forms a plasma to cut the material and utilize robotic assistance for safety and precise repeatability of movements. In contrast, the medical applications using laser systems are mostly driven manually, thermal load is unwanted. The mechanism of action to cut bone with laser differs from the current state of the art cutting tools in such, that the laser is not cutting the bone in one go but ablates the bone layer by layer (approximately 0.3/0.4 mm depth per pulse). In order to reap the advantages of the osteotomy laser (cold, debris free, contact free, free cutting patterns) it must be coupled to a robot. Operating the laser by hand does not achieve the required accuracy needed for an efficient use of the tool and an acceptable cutting width – functional cuts are not possible at all. However, the robot must not hinder the surgeon during the intervention and the system must allow for a “single lot” planning as each patient is different.

The CARLO® device combines robotic accuracy, the advantages of laser as a cutting tool and the possibility of easy “single lot” preoperative planning in one device. The Er:YAG laser source

provides the optimal wavelength to ablate bone and is hence best suited for building a miniaturized laser head which can be mounted onto the distal end of a tactile, relatively small surgical lightweight robot using up as little space as possible. In our study, the CARLO<sup>®</sup> device has shown in a near identical operation theatre environment, that preoperative planning based on CT data can be precisely executed. The high cutting precision could be demonstrated in various indications using functional cuts. The functional cuts lead to an easy reconstruction situation of the defect and a load bearing situation which would allow minimizing the amount of osteosynthesis material to be used for the trauma (it might even be possible to use resorbable material instead of metal implants). Other advantages using this technique are the omission of a cutting guide/template and the turnaround time for preparing the tool for upcoming interventions due to its contactless cutting mechanism. Besides the cost for the cutting templates, the templates might even render a lesser outcome accuracy than the laser due to possible planning failures, fabrication errors a mispositioning of the templates during the operation or if the local anatomy is not adequately represented in the planning steps. Another indication in tumor surgery of the mouth floor is the median mandibular split with a wave-shaped cut design. The advantage of a precise repositioning of the osteotomized mandibular edges is subsequently made possible. Likewise, the split osteotomy a sinusoidal cut geometry of 5mm width and 5mm amplitude in Le Fort I level bilaterally for the subsequently down fracture of the maxilla was done. In an easy way, an offset positioning of the maxilla can be achieved by the width of the cuts. Thanks to the interlocking faces of the maxilla to the midface complex a higher stability but also a higher accuracy of the maxillary movement can be reached in an easy matter. In correction or access osteotomies, a narrow bone cutting width of only a few hundred microns is desirable. Further, the cut should not only be narrow but also congruent to the preoperative plan. Achieving this manually is beyond human capabilities – or at least very difficult. Conventional manually guided cutting instruments, for example piezoelectric devices, have instruments resulting in cutting widths of about 0.6 mm (Mectron, Italy). The robot guided laser achieves a cutting width of 0.5 mm and was exactly congruent to the preoperative planning. A recent histological comparison study indicates the highest bone cut precision for laser osteotomies<sup>9</sup>. Combining the benefits of the osteotomy laser (cold, debris free harvesting channels) with the robotic feature (tactile, precise, free cutting patterns) new possibilities for osteotomies arise. Last, but certainly not least, the contactless of the laser offers a relevant and important safety feature. When moving the cadavers during the study, the cutting laser stopped immediately, the system aligned itself to the preoperatively defined cutting path (latency of the robot), and, once aligned, continued to ablate. As no physical instrument had to be retracted from the corps, no damage was assessed. In all tests, no carbonization or smear layers were seen macroscopically. One reason for this is the highly focused emitted energy of the Er:YAG laser to a very small area of bone. The watery content

of the bone is heated up quickly, leading to a small “micro explosion” (Burgner et al. 2010) and a kinetic charge to the bony debris which is ejected. The sum of the “micro” explosions results in a debris free and open porous cutting face. The water content in bone tissue is 23.5 % for cortical bone and 30.5 % for trabecular bone respectively (Afzal 2004). Previous studies have shown that the Er:YAG laser, with its wavelength of  $\lambda=2,94 \mu\text{m}$ , has a strong absorption coefficient for water. In addition, the organic matrix and inorganic calcium salts, the major component found in bone, also have a very high absorption coefficient for Er:YAG laser irradiation (Bayly et al. 1963, Doyle et al. 1975, Miller 1952). As a result, Er:YAG laser ablates bone efficiently (Hibst 1992) and a propagation of heat to the surrounded bony tissue is very limited. The capability of the Er:YAG laser to perform efficient and carbonization free osteotomies, has been shown previously in a variety of non-clinical studies (Akyol et al. 2009, Kan et al. 2008, Buchelt et al. 1994, Matys et al. 2016, Romeo et al. 2009). The narrow cutting width down to  $500 \mu\text{m}$ , and thereby the reduced bone loss, allow a faster bone healing as two animal studies by the authors (Augello et al. 2017, Augello et al. 2017) proved in  $\mu\text{CT}$ -scan and histological examinations. The bone healing in these studies were not impaired but even accelerated after Er:YAG laser irradiation. This may have a significant impact on the healing performance and the pain score and thus leading to a faster, more aesthetic and functional outcome. In contrast to our results, other studies using a  $\text{CO}_2$  laser source showed carbonization of the bony tissue (Kuttenberger et al. 2008, Zhan 2010). The drawback with laser ablation in general, especially in comparison with mechanical cutting instruments, is the relatively low processing/cutting speed. However, CARLO® has shown advantages over the current state of the art cutting tool, e.g. less bone loss, precise and real-time navigated execution of predefined geometries, free osteotomy patterns, and consequently a precise fitting of the graft resulting in a higher primary stability. The slower cutting speed could be balanced by a less time expensive reconstruction/osteosynthesis procedure. With the tactile and contact free osteotomy system, no safety relevant issues could be provoked. Even when moving the specimens significantly and abruptly neither a misfiring of the laser was detected nor any tissue damage detected.

Coupling a miniaturized and robot-guided laser system to a navigation system, as done in the CARLO®, the advantages of performing accurate osteotomies with freely selectable geometries in a safe manner offers new possibilities for patient specific treatment. When using CARLO® in a near operating theatre environment, all interventions could be performed by the surgeon without interfering with their routine. We view the results to be very encouraging and will continue to work with CARLO® on further indications and patient specific osteotomy patterns.

## References

- 1 Zaret MM, Breinin GM, Schmidt H, Ripps H, Siegel IM, Solon LR: Ocular lesions produced by an optical laser. *Science* 134:1525 1526, 1961.
- 2 Taylor R, Shklar G, Roeber F: The Effects of Laser Radiation on Teeth, Dental Pulp, and Oral Mucosa of Experimental Animals. *Oral Surg Oral Med Oral Pathol* 19:786 795, 1965.
- 3 Stuebinger S, Biermeier K, Bachi B, Ferguson SJ, Sader R, von Rechenberg B: Comparison of Er:YAG laser, piezoelectric, and drill osteotomy for dental implant site preparation: a biomechanical and histological analysis in sheep. *Lasers Surg Med* 42: 652 661, 2010.
- 4 Stuebinger S, Kober C, Zeilhofer HF, Sader R: Er:YAG laser osteotomy based on refined computer-assisted presurgical planning: first clinical experience in oral surgery. *Photomed Laser Surg* 25:3 7, 2007.
- 5 Meijer J. Laser beam machining state of the art and new opportunities: *J Mater Process Int J* 149:2 17, 2004.
- 6 Stuebinger, S, Ghanaati S, Saldamli B, Kirkpatrick CJ, Sader R: Er:YAG laser osteotomy: preliminary clinical and histological results of a new technique for contact-free bone surgery. *Eur Surg Res* 42:150 156, 2009.
- 7 Afilal S: Ablationsmechanismen von biologischem Hartgewebe bei Bestrahlung mit kurzgepulsten CO<sub>2</sub>-Lasern. Doctoral dissertation, Heinrich-Heine-University, Düsseldorf, Germany, 2004.
- 8 Burgner J, Mueller M, Raczkowsky J, Woern H: Ex vivo accuracy evaluation for robot assisted laser bone ablation. *Int J Med Robotics Comput Assist Surg* 6:489 500, 2010.
- 9 Rajitha Gunaratne GD, Khan R, Fick D, Robertson B, Dahotre N, Ironside C: A review of the physiological and histological effects of laser osteotomy. *J Med Eng Techn* 41: 1 12, 2017.
- 10 Bayly JG, Kartha VB, Stevens WH: The absorption spectra of liquid phase H<sub>2</sub>O, HDO, D<sub>2</sub>O, from 0.7  $\mu$ m to 10  $\mu$ m. *Infrared Phys* 3:211 223, 1963.
- 11 Doyle BB, Bendit EG, Blout ER. Infrared spectroscopy of collagen and collagen-like polypeptides. *Biopolymers* 14:937 957, 1975.
- 12 Miller GL. Improved infrared photography for electrophoresis. *Science*: 116:687 688, 1952.
- 13 Hibst R: Mechanical effects of erbium:YAG laser bone ablation. *Lasers Surg Med* 12: 125 130, 1992.
- 14 Akyol UK, Guengoermues M, Guendogdu C, Erdem H: Histologic evaluation of the effects of Er: YAG laser on bone ablation. *J Contemp Dent Pract* 10:65 72, 2009.

- 15 Kan HW, Oh J, Welch AJ: Investigations on laser hard tissue ablation under various environments. *Phys Med Biol* 53:3381-3390, 2008.
- 16 Buchelt M, Kutschera HP, Katterschafka T, Kiss H, Lang S, Beer R: Er:YAG and Hol:YAG laser osteotomy: the effect of laser ablation on bone healing. *Lasers Surg Med* 15:373-381, 1994.
- 17 Matys J, Flieger R, Dominiak M: Assessment of temperature rise and time of alveolar ridge splitting by means of Er:YAG laser, piezosurgery, and surgical saw: An ex vivo study. *Bio Med Res Int* 9654975:1-8, 2016.
- 18 Romeo U, Del Vecchio A, Palaia G: Bone damage induced by different cutting instruments – an in vitro study. *Braz Dent J* 20:162-168, 2009.
- 19 Augello M, Deibel W, Nuss K, Cattin P, Juergens P: Comparative microstructural analysis of bone osteotomies after cutting by computer-assisted robot-guided laser osteotome and piezoelectric osteotome. An in vivo animal study. *Laser Med Sci* submitted, 2017.
- 20 Augello M, Deibel W, Plihal H, von Rechenberg B, Cattin P, Juergens P, Nuss P: Effects on bone tissue after a Cold Ablation Robot-Guided Laser Osteotomy on bone healing: An in vivo animal study in sheep. *Int J Oral Maxillofac Surg* submitted, 2017.
- 21 Kuttenger JJ, Stuebinger S, Waibel A, Werner M, Klasing M, Ivanenko M, Hering P, Von Rechenberg B, Sader R, Zeilhofer HF: Computer-guided CO<sub>2</sub>-laser osteotomy of the sheep tibia: technical prerequisites and first results. *Photomed Laser Surg* 26:129-136, 2008.
- 22 Zhan Y: Optimization of pulse distribution for short-pulsed CO<sub>2</sub> laser ablation of bone tissue based on thermal relaxation. Diploma thesis, Karlsruhe Institute of Technology. 2010.

## **5. The use of FEM analysis for modeling different osteotomy patterns and biomechanical analysis of craniosynostosis treatment.**

This part of the thesis focused on more theoretical aspects for an additional indication in the use of the cold-ablation and robot-guided Er:YAG laser osteotome. Namely, the corrective surgery of inborn deformations of the cranial vault (craniofacial surgery in cases of craniosynostosis). Due to premature ossification of cranial sutures, affected children suffer from increased intracranial pressure and additionally present functional and esthetic impairment in the viscerocranium and neurocranium. The state-of-art surgical correction consists of a multi-segmental craniotomy, a deformation, and a re-shaping of the bone flaps, followed by a realignment in a way that allows expansion of the cranial vault according to normal skull dimensions. The bone defect zones should be optimally distributed with regard to the complete new ossification, and proper planning has to involve reference to the underlying viscerocranium and to normal neurocranial dimensions. For this indication, the CARLO<sup>®</sup> prototype could be used to perform the craniotomy with specially calculated cutting geometries in a finite element method analysis and additionally to perform incomplete osteotomies on the inner side of the bone flap to facilitate the re-shaping (skull molding).

This analysis intended to create basic knowledge on the design of different cutting patterns in terms of frequency of the incomplete monocortical cuts, shape of these cuts and allocation of the cuts on the flap to realize the best stress vs. force relation and the most increased projected bone surface.

Project Leaders: Prof. P. Jürgens / Prof. P. Cattin

Publication: First authorship

Accepted in Journal of Craniofacial Surgery, March 11<sup>th</sup> 2019

Impact factor 0.772

Ranking (H-Index) 62

---



# The Use of Finite Element Method Analysis for Modeling Different Osteotomy Patterns and Biomechanical Analysis of Craniosynostosis Correction

Marcello Augello, MD, DDS,\*<sup>†</sup> Manfred M. Maurer, PhD,<sup>‡</sup> Isabelle Berg-Boerner, MD, DDS,<sup>†§</sup>  
Hans-Florian Zeilhofer, MD, PhD,<sup>†§</sup> Philippe Cattin, PhD,<sup>||</sup> and Philipp Juergens, MD, DDS<sup>†§</sup>

**Purpose:** Several post-processing algorithms for 3D visualization of the skull in craniosynostosis with their specific advantages and disadvantages have been already described. The Finite Element Method (FEM) described herein can also be used to evaluate the efficacy of the cutting patterns with respect to an increase in the projected surface area under assumed uniform loading of the manipulated and cut bone segments.

**Methods:** The FEM analysis was performed. Starting with the classic cranial osteotomies for bifrontal craniotomy and orbital bandeau a virtually mirroring of the unaffected triangular shaped frontal bone was performed to achieve a cup-shaped sphere of constant thickness of 2.5 mm with a radius of 65 mm. Mechanical properties required for the analysis were Young's modulus of 340 MPa and Poisson's ratio of 0.22. Four different cutting patterns from straight to curved geometries have been projected onto the inner surface of the sphere with a cutting depth set to 2/3rds of the shell thickness. The necessary force for the deformation, the resulting tensions and the volume loss due to the osteotomy pattern were measured.

**Results:** Better outcomes were realized with pattern D. The necessary force was 73.6% smaller than the control group with 66N. Best stress distribution was achieved. Curved cutting patterns led to the highest peak of stress and thus to a higher risk of fracture. Straight bone cuts parallel to the corners or to the thighs of the sphere provided a better distribution of stresses with a small area with high stress. Additionally, also with pattern D a surface increase of 20.7% higher than reference was registered.

**Conclusion:** As a proof of concept for different cutting geometries for skull molding in the correction of craniosynostosis, this computational model shows that depending of the cutting pattern different biomechanical behavior is achieved.

**Key Words:** Craniosynostosis, FEM analysis, skull molding

(*J Craniofac Surg* 2019;30: 1877–1881)

Craniosynostosis is a relatively rare congenital malformation of the skull resulting from the premature fusion of one or more cranial sutures. The incidence rate of craniosynostosis is reported to be 1/2100 to 2500 births.<sup>1–3</sup> Non-syndromic craniosynostosis or isolated forms represent 85% of the cases.<sup>4</sup> In normal development, cranial growth takes place perpendicular to the suture lines leading to a well-proportioned head with a longer anteroposterior than bitemporal dimension.<sup>5</sup> Premature fusion of one or more sutures precludes the growth of cranial bones perpendicular to the affected sutures and leads to compensatory growth in a parallel direction, resulting in a cranial dysmorphic head shape.<sup>6</sup> The main purpose of correction of a craniosynostosis skull is to re-open the cranial sutures with bone slots to free the skull bones and allow proper brain development inside.

The surgical correction of craniosynostosis is complex and represents an interdisciplinary challenge, as the procedure is comparatively rare even at specialized centers.<sup>7</sup> As early surgery is beneficial, there is a demand for less invasive but effective techniques. Among other issues, surgical time, and blood loss are of importance in the small children undergoing surgery. Different surgical techniques, variations in the shape of the osteotomies, and fixation of the osteotomy segments for remodeling have been described and compared for different patient groups. Furthermore, alternative approaches, including distraction and other techniques, have been reported.<sup>8–10</sup> Several post-processing algorithms for 3D visualization of the skull in craniosynostosis have been described, each with specific advantages and disadvantages.<sup>11</sup> Alternative techniques using image data for surgical planning include stereolithographic modeling and computer-assisted surgical planning.<sup>12</sup> Thus, craniosynostosis corrections are preoperatively planned with a 3D tool to obtain an individual 3D model; afterward, bone flaps are created with surgical guides.<sup>13</sup> Currently, the inner layer of the bone flaps is not osteotomized, so that the deformation of the flaps is more random, which reduces the precision of the procedure. It remains unclear whether an internal osteotomy with predefined patterns enfeebls the bone in a way that it can be deformed with an optimal stress distribution and an enlargement of the flap's surface.

To gain basic knowledge about the different geometries of the osteotomy pattern in term of frequency, shape, and allocation, as well as the resulting biomechanical behavior of stress and forces, here we evaluate the relationship between various osteotomies patterns and the skull bone rigidity using Finite Element Method (FEM) analysis.

## METHODS

The correction of complicated skull deformations must be planned individually for each patient. For the FEM analysis in this study, the

From the \*Department of Cranio-Maxillofacial Surgery, Hospital Aarau, Aarau; <sup>†</sup>Hightech Research Center of Cranio-Maxillofacial Surgery, University of Basel, Allschwil; <sup>‡</sup>CAD/FEM (Suisse) AG, Aadorf; <sup>§</sup>Department of Cranio-Maxillofacial Surgery, University Hospital, Basel; and <sup>||</sup>Department of Biomechanical Engineering, University of Basel, Allschwil, Switzerland.

Received January 22, 2019.

Accepted for publication March 11, 2019.

Address correspondence and reprint requests to Dr Marcello Augello, MD, DDS, Department of Cranio-Maxillofacial Surgery, Telstrasse 21, 5001 Aarau, Switzerland; E-mail: marcello.augello@ksa.ch

PC and PJ equally contributed to this paper.

The authors report no conflicts of interest.

Copyright © 2019 by Mutaz B. Habal, MD

ISSN: 1049-2275

DOI: 10.1097/SCS.00000000000005579

*The Journal of Craniofacial Surgery* • Volume 30, Number 6, September 2019

1877

Copyright © 2019 Mutaz B. Habal, MD. Unauthorized reproduction of this article is prohibited.

## Abstract

**Objective:** Several post processing algorithms for 3D visualization of the skull in craniosynostosis with their specific advantages and disadvantages have been already described. The FEM described herein can also be used to evaluate the efficacy of the cutting



patterns with respect to an increase in the projected surface area under assumed uniform loading of the manipulated and cut bone segments.

**Methods:** FEM analysis was performed. Starting with the classic cranial osteotomies for bifrontal craniotomy and orbital bandeau a virtually mirroring of the unaffected triangular shaped frontal bone was performed to achieve a cup-shaped sphere of constant thickness of 2.5 mm with a radius of 65 mm. Mechanical properties required for the analysis were Young's modulus of 340 MPa and Poisson's ratio of 0.22. Four different cutting patterns from straight to curved geometries have been projected onto the inner surface of the sphere with a cutting depth set to 2/3 rds of the shell thickness. The necessary force for the deformation, the resulting tensions and the volume loss due to the osteotomy pattern were measured.

**Results:** Better outcomes were realized with pattern D. The necessary force was 73.6 % smaller than the control group with 66 N. Best stress distribution was achieved. Curved cutting patterns led to the highest peak of stress and thus to a higher risk of fracture. Straight bone cuts parallel to the corners or to the thighs of the sphere provided a better distribution of stresses with a small area with high stress. Additionally, also with pattern D a surface increase of 20.7 % higher than reference was registered.

**Conclusion:** As a proof of concept for different cutting geometries for skull molding in the correction of craniosynostosis, this computational model shows that depending of the cutting pattern different biomechanical behavior are achieved.

## Introduction

Craniosynostosis are relatively rare congenital malformations of the skull resulting from the premature fusion of one or more cranial sutures. The incidence is reported to be 1/2'100 – 2'500 births.<sup>1-3</sup> Non-syndromic craniosynostosis or isolated forms represent 85 % of the cases.<sup>4</sup> In normal development, cranial growth takes place perpendicular to the suture lines leading to a well-proportioned head with a longer anteroposterior than bitemporal dimension.<sup>5</sup> Premature fusion of one or more sutures precludes the growth of cranial bones perpendicular to the affected sutures and leads to compensatory growth in a parallel direction, resulting in a cranial dysmorphic head shape.<sup>6</sup> The main purpose of correction of a craniosynostosis skull is to re-open the cranial sutures with bone slots to free the skull bones and allow proper brain development inside. The surgical correction of craniosynostosis is complex and represents an interdisciplinary challenge, as the procedure is comparatively rare even at specialized centers.<sup>7</sup> As early surgery is beneficial, there is a demand for less invasive but effective techniques. Among other issues, surgical time and blood loss are of importance in the small children undergoing surgery. Different surgical techniques, variations in the shape of the osteotomies and fixation of the osteotomy segments, for remodeling have been described and compared for different patient groups. Furthermore, alternative approaches, including distraction and other techniques have been reported.<sup>8-10</sup> Several post processing algorithms for 3D visualization of the skull in craniosynostosis with their specific advantages and disadvantages have been described.<sup>11</sup> Alternative techniques using image data for surgical planning include stereolithographic modeling and computer-assisted surgical planning.<sup>12</sup> Thus, craniosynostosis corrections are preoperatively planned with a 3D tool to obtain an individual 3D model, afterwards bone flaps are created with surgical guides.<sup>13</sup> Nowadays, the inner layer of the bone flaps is not osteotomized, so that the flaps deformation is more randomly being a drawback in terms of precision. The question is whether an internal osteotomy with predefined patterns enfeebls the bone in a way that it can be deformed with an optimal stress distribution and an enlargement of the flap's surface.

To get basic knowledge on the different geometries of the osteotomy pattern in term of frequency, shape and allocation with the resulting biomechanical behavior of stress and forces this investigation intends to evaluate the relationship between various osteotomies patterns and the skull rigidity using Finite Element Method (FEM) analysis.

## Materials and Methods

The correction of complicated skull deformations must be planned individually for each patient. For the FEM analysis in this study, the skull of a 14-month-old boy was selected. The child suffered from an anterior plagiocephalus. The standard surgical approach in our department provides a frontoorbital advancement.<sup>14</sup> Local institutional review board approved this study. Surgical planning involved a thin-cut CT scan of 0.35 mm isotropic resolution (GE Medical Systems Bright Speed S scanner) with 3D reconstructions of the head to evaluate the craniosynostosis. For the reconstruction, 234 slices in the transversal plane were used. The DICOM data set was imported and 3D reconstructed using the software SurgiCase-CMF (version 5.0, Materialise, Belgium). After visualization of the skull morphology, the 3D virtual planning was performed. The procedure started by outlining the classic cranial osteotomies for bifrontal craniotomy and orbital bandeau. By virtually mirroring the patient's unaffected side, the changement of the frontal part with mostly a triangular shape was adjusted. Obviously, due to the not accurate fitting of the bone pieces', gaps in between remain (Figure 1).

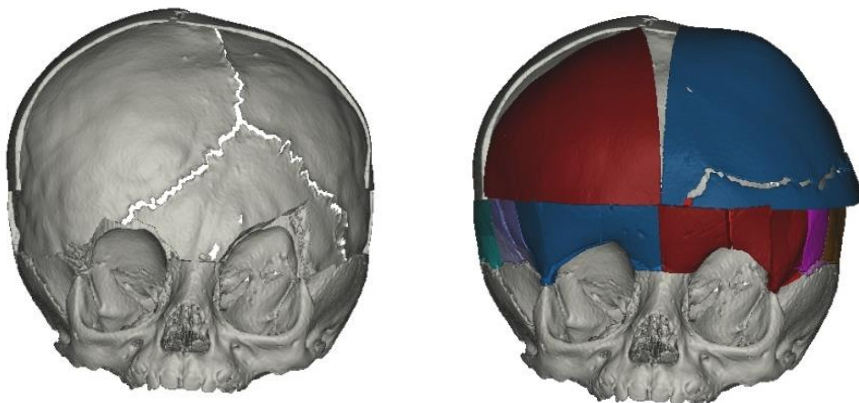


**Figure 1:** 3D reconstruction of an anterior plagiocephalus with virtual surgical planning.

From this triangular bone piece, a cup-shaped sphere was calculated (Figure 2). The proposed finite element model and its biomechanical analysis with ANSYS® Version 19 (ANSYS® Inc., Canonsburg, U.S.) was based on a reconstructed shape of a spiky shell of constant thickness of 2.5 mm and a radius of 65 mm. To facilitate the investigation of the biomechanical response to the varying cutting geometries the orbital bandeau due to the irregular thickness was not included.

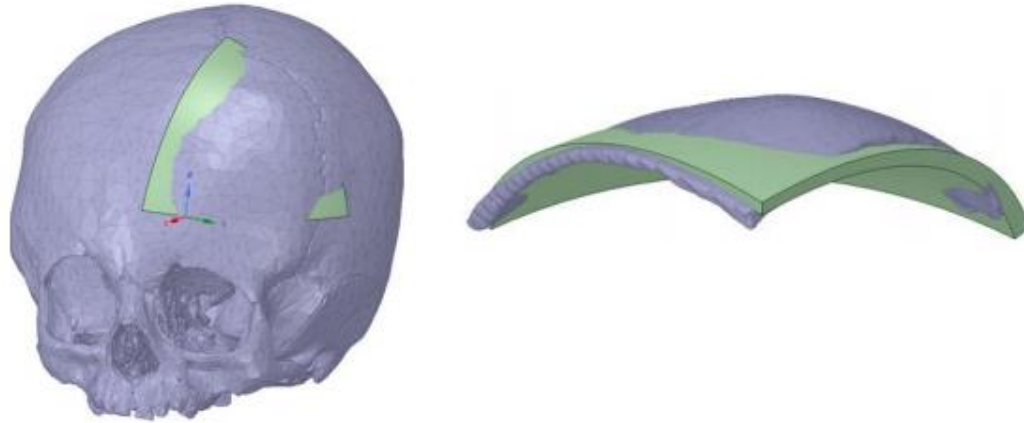


**Figure 2:** From the triangular frontal bone segment (grey) a cup-shaped sphere (green) of similar volume was calculated. Radius Reference = 70.5 mm, Radius Reconstructed body = 68 mm, Thickness = 2.5 mm.

The parameters for the given volume were chosen to objectify the data as much as possible. The frontal skull bones were defined as a linear-elastic, isotropic and homogenous material behavior of a 1.5-year-old child. Homogenous due to the same mechanical properties in all their points, isotropic, because in all points the mechanical properties do not change with direction, and linear elastic because they return to the original shape when tension is removed.<sup>15</sup> The necessary mechanical properties required for this analysis are Young's modulus of 340 MPa as the median value of several studies<sup>16-19</sup> and Poisson's ratio of 0.22. A finite element mesh of 346'943 nodes and 220'294 elements could be calculated as shown as an example of reference sphere (Figure 3). The FEM mesh was chosen in a way such that 2-3 elements were across the thickness in each area in order to be able to reproduce accurately the stress gradient. According to the virtual skull of the anterior plagiocephalus the skull thickness measured 2.5 mm. The different cutting patterns have been projected onto the inner surface of the sphere (Figure 4). The projection does not follow the curvature of the sphere and thus remains vertical. The cutting depth has been set to 2/3 rds of the shell thickness, with 1/3 remaining whole.



**Figure 3:**

A finite element mesh could be calculated as shown. At least 2-3 elements were across the thickness in each area to be able to reproduce accurately the stress gradient.

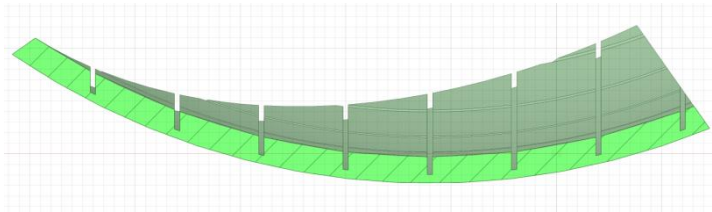


**Figure 4:**

The different patterns were projected in a vertical direction on the inside of the body. 2/3<sup>rd</sup> of the thickness was cut, leaving 1/3<sup>rd</sup> material left.

The upper edge segment of corner (a) of the cutout was set at the equivalent to the outer bone layer not to be cut by the laser beam. This corner was thus fixed. The inner part of corner an ensured the free movement, allowing the expansion of the sphere towards a flat surface (Figure 5). The necessary force for the deformation of the sphere, the resulting tensions and the volume loss due to the osteotomy pattern were measured.

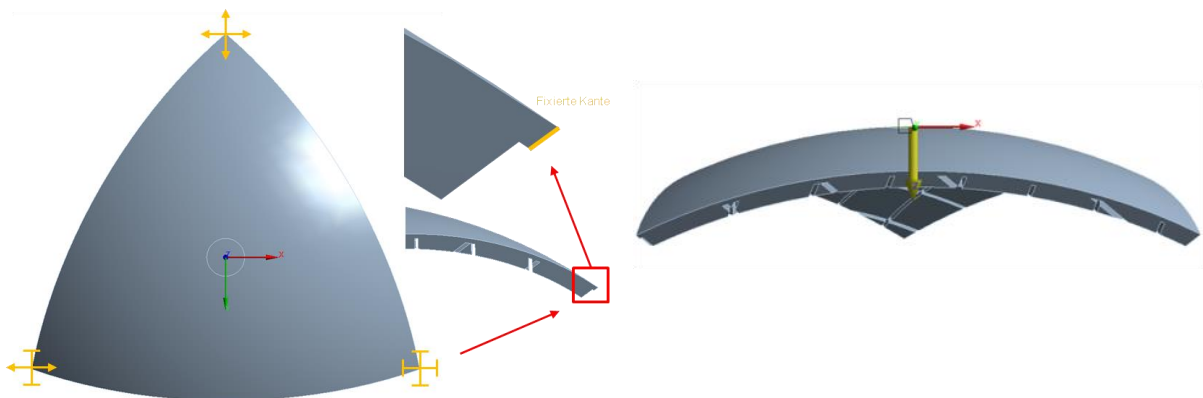


**Figure 5:** The upper edge segment of corner (a) was fixed. Corners (b) and (c) were free for free for expansion. The body was pressed downwards for 5 mm.

It was started with a checkerboard-like pattern. The cutting width of 0.5 mm was ideally planned for the intended use of a laser beam such as the cold ablation and robot-guided laser osteotome CARLO®.<sup>20</sup> The distance between the osteotomy lines and the outer apex of the sphere was virtually pressed downwards by 5 mm. The second cut pattern had a central circle of 10 mm, and of this, to the edges radiating osteotomies with 15 ° interval obtaining bisecting osteotomies in the corner. After analyzing the resulting stresses and the force needed to deform the sphere, circular osteotomies from the edges to the center were chosen. The bisecting osteotomies were still done. Finally, the last pattern represented an optimization of all osteotomy designs. Straight, parallel cuts to the corners from a centrally positioned triangle with a side length of 10 mm were made (Figures 6a-d). All measured values were compared to the uncut sample.

The models were evaluated according to the main tension using a ration in MPa (N/mm<sup>2</sup>). The tension fields were evaluated using von Mises analysis (average stress level). A color scale with tension values varying in MPa was used and each color map presented a specific scale according to the result under study. After biomedical analysis of the results, the tested cutting designs were compared verifying the tendencies of behavior of the different pattern considering the distribution of tension.

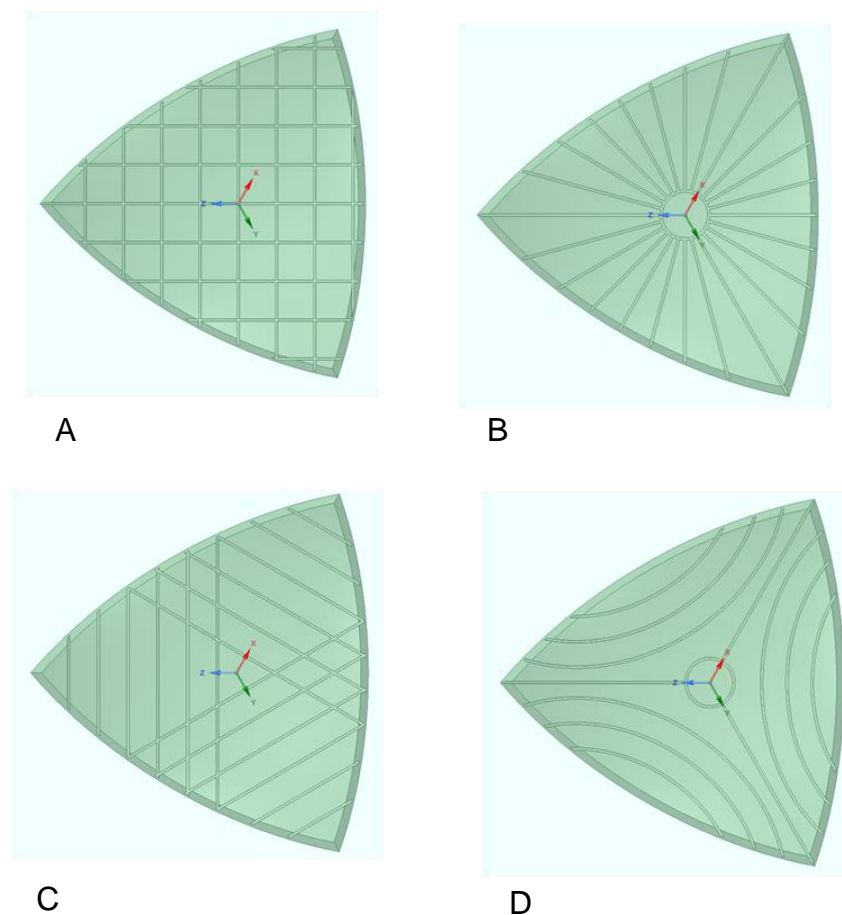


**Figure 6:**  
Different cutting designs of  
the inner layer of the spheres.

## Results

To allow a comparison of the different patterns, the shape and the thickness of the reconstructed sphere was identical for all tests. As well all cuts were performed with the same depth.

The non-osteotomized sphere represented the control group with a volume of 7736.9 mm<sup>3</sup>. To deflect it 5 mm downwards 250 N force was needed. The highest tension peaks up to 80 MPa were measured in the edges of the sphere and about half of the maximal tension in the middle area. The biomechanical analysis rendered the color map of stress that occurred during the deflexion simulation as shown in the Figures 7a-e. Despite similar volume reductions in all cut designs (6.84-8.24 %, Table 1), there were differences in the mechanical response in terms of force reaction and stress.

Osteotomies weaken the bone and, as expected, considerably lower forces were needed than in the control body to deflect the sphere. With pattern D, the necessary force was even 73.6 % smaller than in the control group, meanwhile in osteotomy design C a 3 times greater force was needed for the same bend comparing the osteotomy pattern D, 66 N vs. 177 N.

The mechanical evaluation of the sphere deflexion demonstrated that the values of von Mises stress were higher for all tested patterns than in the control group. Osteotomy design A showed the highest stress with 135 MPa in the area of the corners and tangential to it. Whereas the osteotomy design B, showed a higher overall stress distribution above the sphere than the other three tested bodies and the control body. The lowest stress distribution showed pattern D. Compared to the control group all von Mises stress values were higher. In principle, the results showed that curved patterns led to highest peak of stress in these regions and thus to a higher risk of fracture. On the contrary, straight bone cuts parallel to the corners or to the thighs of the sphere provided a better distribution of stresses with a small area with high stress. The computational model described herein was also used to evaluate the efficacy of the cutting patterns with respect to an increase in the projected surface area under assumed uniform loading of the manipulated and cut bone segments. While the total increase in the area was rather small (around 2 %), it was still possible to make a relative comparison of the cutting patterns. And in fact, again pattern D shows the largest increase in projected surface area compared to the reference model with no cutting pattern (20.7 % higher area increase compared to the reference, table 2). Figure 8 shows the undeformed reference (no cutting pattern, red) overlaid with the deformed pattern D (yellow) as seen from straight above the bone segments. The net increase in the covered area is clearly visible.



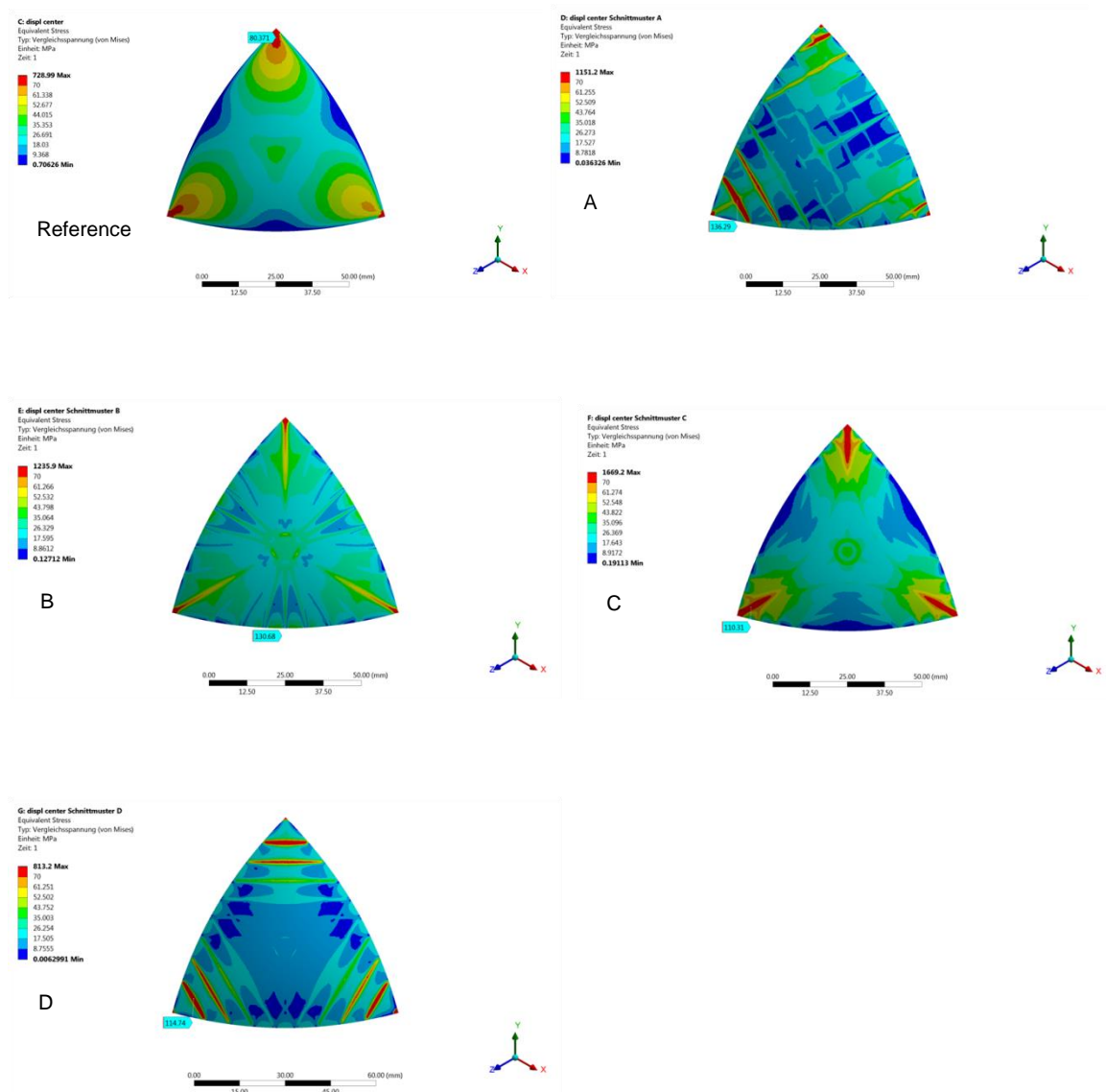


**Figure 7a-e:** The biomechanical analysis of the different cutting designs rendered the color map of after deflexion

Design	Volume (mm <sup>3</sup> )	%	Force (N)	%	Stress (MPa)	%
Reference	7736.9	100	250	100	80	100
A	7099.6	91.76	84	33.6	135	168.75
B	7174.9	92.74	113	45.2	130	162.5
C	7207.4	93.16	177	70.8	110	137.5
D	7175	92.74	66	26.4	115	143.75

**Table 1:** Summary of volume reduction, needed bending force and stress for the control group and the four cutting geometries.



<b>Volume</b>	<b>Projected area</b>	<b>Change compared to undeformed state</b>	<b>Change compared to deformed reference</b>
	[mm <sup>2</sup> ]	[%]	[%]
<b>Undeformed</b>	3086		
<b>Reference (deformed, no pattern)</b>	3144	1.9	
<b>Pattern A</b>	3151	2.1	12.1
<b>Pattern B</b>	3154	2.2	17.2
<b>Pattern C</b>	3139	1.7	-8.6
<b>Pattern D</b>	3156	2.3	20.7

**Table 2:** Changing surface areas depending on the different cutting pattern compared to the undeformed and not osteotomized body.

## Discussion

The surgical correction of craniosynostosis is a time-consuming and a complex challenge. The difficulty of correction relates to the proper position of the frontal bone and particularly to the orbital bandeau. Besides, surgeons wish to get an effective technique to decrease the procedure time and to facilitate the surgery. Virtual models and pre-operative planning would allow surgeons to predict the effects of a surgery and to avoid undesired complications such as bone fractures. Virtual models give a better visualization of the skull deformation. Cutting guides are helpful for surgery to shape the planned bone flaps. But to enfeeble the flap in a determined form is still a challenge. According to our experience the bone in children between one and two years is more brittle, making bending less effective. Thereby, the usual osteotomy of the cranial vault leaves defects between the bone segments that tend to be larger at this age. These children usually require bone grafting as suggested in studies by Grant et al.<sup>20</sup>, Cohen et al.<sup>21</sup>, and Gao et al.<sup>22</sup>. As in the described technique by Cohen et al. they used onlay grafts to augment the deficient bone of the brow region to bring forward the entire frontal bone segment from the bifrontal craniotomy. They describe as a disadvantage of repositioning this large bone flap is a loss of flexibility in reshaping the forehead. Already selective weakening of the bone by the placement of channels or kerfs in the inner layer of the bone flaps are performed trying to get around this problem<sup>23</sup>. In the study of Gao et al. bone graft was obtained from the endocortex of the removed bone segments or the ectocortical surface of intact bone. Two groups of different ages were examined. Mean age at time of procedure for group 1 was 12.2 months and for group 2 20.2 months. At final follow-up in group 1 the residual osseous defect was 33.3 % vs. 7.9 % of group 2 with a need of cranioplasty of 26.7 % vs. 5.3 %. Alternative to manage large residual cranial defects is the use of some type of alloplastic or osteoinductive materials which are expensive. Also, the overcorrection of the orbital bandeau advancement by Taylor et al.<sup>24</sup> was proposed. In a large cohort study of 207 patients with isolated synostosis the traditional fronto-orbital advancement and cranial vault remodeling with overcorrection of the bandeau were performed to overcome the problem of a relapse. The follow up of five years and more showed cases of supraorbital retrusion and temporal hollowing, hallmarks of poor aesthetic outcomes.

Therefore, efforts are made by various groups of surgeons to optimize the correction technique getting not always satisfactory results. Plausible would also seem to mold bone flap in a predefined shape to obtain a more predictable surface. In fact, a pre-operative corrected 3D model of the forehead / orbital bandeau could be used as a template to mold the weakened bone flap by a specific osteotomy pattern on the inner bone table. For this approach the biomechanical behavior of different cutting patterns should be investigated. The cutting geometry of the inner layer of a bone flap is nowadays still a challenge hampered by the bound

to the common tools such as a drill or piezo osteotome. The disadvantage of mechanical instruments is as known the difficulty of control doing fine, intricate, nonlinear cuts problematic. This issue can be circumvented by using a computer-assisted and robot-guided laser source for osteotomies.<sup>25</sup> As already known, with a laser osteotome freely selectable osteotomy patterns can be performed,<sup>26</sup> but this topic was not subject of our investigation. Additionally, to the geometry of the cutting patterns also the depth of the cut is important, which remains uncontrolled by using hand-driven osteotomy tools.

The Finite Element Method is widely used in biomechanical investigations, but the preoperative planning with the FEM analysis, especially for craniosynostosis surgery is still not very popular. The cranium mechanics simulation during craniosynostosis correction treatment shows that the engineering support in planning is very important to obtain the optimal effects of the surgery. Moreover, pre-operative planning allows constructing a patient-specific treatment, by choosing the number and the location of the cuts and then by predicting the effect of the correction and deformation of the flap. Thus, the optimal surgery can be constructed. Unfortunately, only few material properties are available in the literature for infant cranial bones. Therefore, this study had to be conducted with some approximations. First, the approximation of an isotropic bone tissue was made. However, several studies reveal that properties of bone depend on the orientation of load.<sup>27-29</sup> Mechanical tests should be performed with human child skulls to determine properties in different configurations, which is not realizable from an ethical point of view. In craniosynostosis, surgeons must work on other cranial bone such as the parietal or occipital bone. The occipital bone was found to be thicker than the parietal and frontal bones.<sup>30,31</sup> To get an accurate simulation, the mechanical properties and the thickness of the other cranial bones should precisely be determined. As many previous related studies, which aimed at developing FEM models of child skull, this study assumed the skull thickness to be constant. Indeed, the skull thickness is set to 4mm for a three-year-old child and to 1.4 mm for a newborn in the models developed by Roth et al..<sup>32</sup> Similarly, a constant skull thickness of 2.5 mm was assumed in this study. It should be stressed that the variation of the skull thickness must be considered before choosing the cutting depth of the patterns. Despite the fact, that there are some limitations, these investigations demonstrate that it is very important for the surgeon to have optimal osteotomy patterns in order to manipulate efficiently the bone flaps in craniosynostosis cases. With a FEM analysis and the simulation of different cutting patterns presented in this study, we could show the biomechanical responses to a deflection of 5mm with the intention to verify if the bone flap can be weakened in a way that it can be bent without fracture it. Our results demonstrated that with the osteotomy pattern D, straight cuts parallel to the corners and to the thighs of the sphere, only needed a quarter of the force as for the same bend as the untreated model. Only slightly higher stress values in the edge regions were measured for pattern D compared to the

reference model but with a better stress distribution. The pattern D showed an over-expansion of the surface area of 20.7 % compared to the reference, which correspond to an overcorrection. However, a high number of cuts can lead to the disadvantage that the infant's skull could also permanently be weakened, which should be avoided. Curved cuts seem not to be more advantageous. Thus, the analysis enabled to ensure that for our tested cutting designs the best was variant D, because the criteria of minimizing the bending force with a good stress distribution with no fracture to attain the optimal bone flap deformation were satisfied.

Thinning of the bone flap by cutting the inner layer bone in a selected geometry influence the tension forces on the bone flap itself and affect the final molding. Because this study was done as a proof of concept, the orbital dysmorphology, particularly regarding the sphenoid dysplasia and lateral orbital wall defining characteristics of the deformity and the bandeau were not included in this investigation. Having obtained promising results in a following analysis, we will assess the different osteotomy designs for the orbital pillar and tenon segments as maybe the key to achieve acceptable aesthetic results. As well a cadaver study with a cold-ablation and robot-guided laser osteotome<sup>26</sup> to evaluate the efficacy of these FEM models for clinical practice will be performed.

The pre-operative virtual planning allows the surgeons to predict the effects of the treatment. Virtual planning of the treatment is helpful, because it helps to practice patient specific incisions before the real-life surgery and to ensure the optimal solution for cutting pattern attaining a moldable bone segment minimizing incisions and minimizing stress. We are aware that this method shows not the final correction of a unilateral synostosis correction but intended to get knowledge about the biomechanical behavior of different osteotomy geometries on the endocortex. In this regard, further studies, particularly with biological specimens to verify the theoretical outcomes are necessary.

## **Conclusion**

Virtual models permit better visualization of a problem in individual cases. The here presented FEM analysis proposes a tool that evaluates the most appropriate cutting geometry on the inner layer of a bone flap based on calculated stresses and forces reaction to allow a predictable bone molding. These results may provide a first knowledge about the mechanical behavior of different osteotomy geometries.

## Literature

1. Johnson D, Wilkie AOM: Craniosynostosis. *Eur J Hum Genet* 2011;19(4):369–76.
2. Lajeunie E, Le Merrer M, Bonaiti-Pellie C, Marchac D, Renier D: Genetic study of nonsyndromic coronal craniosynostosis. *Am J Med Genet.* 1995;55(4):500–4.
3. Wilkie AOM, Byren JC, Hurst JA, Jayamohan J, Johnson D, Knight SJL: Prevalence and Complications of Single-Gene and Chromosomal Disorders in Craniosynostosis. *Pediatrics* 2010;126(2):e391–400.
4. Boyadjiev SA: Genetic analysis of non-syndromic craniosynostosis. *Orthod Craniofacial Res.* 2007;10(3):129-137.
5. Ciurea A V, Toader C: Genetics of craniosynostosis: review of the literature. *J Med Life* 2008;2(1):5–17.
6. Badve CA, Mallikarjunappa MK, Iyer RS, Ishak GE, Khanna PC: Craniosynostosis: Imaging review and primer on computed tomography. *Pediatric Radiology* 2013;43(6):728–42.
7. Hicdonmez T, Parsak T, Cobanoglu S: Simulation of surgery for craniosynostosis: a training model in a fresh cadaveric sheep cranium. Technical note. *J Neurosurg* 2006;105:150–152.
8. Akai T, Iizuka H, Kawakami S: Treatment of craniosynostosis by distraction osteogenesis. *Pediatr Neurosurg* 2006;42:288–292.
9. Erdinciler P, Kaya AH, Kafadar A, Canbaz B, Kuday C: Bilateral peninsula-shaped linear craniectomy for mild degrees of craniosynostosis: indication, technique and long-term results. *J Cranio-Maxillo-Facial Surg* 2004;32:64–70.
10. Girod S, Teschner M, Schrell U, Kevekordes B, Girod B: Computer-aided 3-D simulation and prediction of craniofacial surgery: a new approach. *J Cranio-Maxillo-Facial Surg* 2001;29:156–158.
11. Levi D, Rampa F, Barbieri C, Pricca P, Franzini A, Pezzotta S: True 3D reconstruction for planning of surgery on malformed skulls. *Childs Nerv Syst* 2002;18:705–706.
12. Medina LS, Richardson RR, Crone K: Children with suspected craniosynostosis: a cost-effectiveness analysis of diagnostic strategies. *Am J Roentgenol* 2002;179:215–221.
13. Rodt T, Schlesinger A, Schramm A, Diensthuber M, Rittierodt M, Krauss JK: 3D visualization and simulation of frontoorbital advancement in metopic synostosis. *Childs Nerv Syst* 2007;23:1313-1317.
14. Voth D, Schwarz M, Wagner W, von Domarus H, Henn M, Schweden F: The frontoorbital advancement – on the use of 3D-CT and the miniplate osteosynthesis. *Neurosurg Rev.* 1992;15(3):209-215.

15. Beer FP, Johnston ER, Dewolf JT, Mazurek DF: Mechanics of materials, 6<sup>th</sup> ed. New York: McGraw-Hill:2012.
16. Couper ZS, Albermani FG: Biomechanics of shaken baby syndrome: physical testing and numerical modeling. In Developments in Mechanics of Structures and Materials, Vol 1, Deeks & Hao (eds.). Taylor & Francis Group: London, 2005;213-218.
17. Coats B, Margulies S: Material properties of human infant skull and suture at high rates. J Neurotrauma 2006; 23(8):1222-1232.
18. Baumer TG, Powell BJ, Fenton TW, Haut RC: Age dependent mechanical properties of the infant porcine parietal bone and a correlation to the human. Biomech Eng 2009;131(11):111-116.
19. Gzik M, Wolanski W, Tejszerska D, Gzik-Zroska B, Kozlak M, Larysz D, Mander M: Application of 3D modelling and modern visualization technique to neurosurgical trigonocephaly correction in children. World Congress on Medical Physics and Biomedical Engineering. Munich, Germany. IFMBE Proceedings 2009;25(9):68-71.
20. Grant III JH, Roberts TS, Loeser JD, Gruss JS: Onlay bone graft augmentation for refined correction of coronal synostosis. Cleft Palate Craniofac J 2002;39(5):546-554.
21. Cohen SR, Kawamoto HK, Burstein F, Peacock WJ: Advancement-onlay: an improved technique of fronto-orbital remodeling in craniosynostosis. Childs Nerv Syst 1991;7:264-271.
22. Gao LL, GF Rogers, Clune JE, Proctor MR, Meara JG, Mulliken JB, Greene AK: Autologous cranial particulate bone grafting reduces the frequency of osseous defects after cranial expansion. J Craniofac Surg 2010;21:318-322.
23. Persing JA, Luce C: Remodeling techniques for immature and mature cranial vault bone: technical note. J Craniofac Surg 1990;1(3):147-149.
24. Taylor JA, Paliga JT, W AM, Tahiri Y, Goldstein JA, Whitaker LA, Bartlett SP: A critical evaluation of long-term aesthetic outcomes of fronto-orbital advancement and cranial vault remodeling in nonsyndromic unicoronal craniosynostosis. Plast Reconstr Surg 2015;13(5):220-231.
25. Deibel W, Schneider A, Augello M, Bruno A, Juergens P, Cattin P: A compact, efficient, and lightweight laser head for CARLO: integration, performance and benefits. Proceedings of SPIE 2015;9579:957905.
26. Augello M, Baetscher C, Segesser M, Zeilhofer HF, Cattin P, Juergens P: Performing partial mandibular resection, fibula free flap reconstruction and midfacial osteotomies with a cold ablation and robot-guided Er:YAG laser osteotome (CARLO®) – A study on applicability and effectiveness in human cadavers. J Craniomaxillofacial 2018;46(10):1850-1855.

27. Currey JD: The effect of porosity and mineral content on the Young's modulus of elasticity of compact bone. *J Biomech* 1988;21:131-139.
28. Martin RB. Determinants of the mechanical properties of bones. *J Biomech* 1991 24 (Suppl. 1):79-88.
29. Schaffler MB, Burr DB: Stiffness of compact bone; effects of porosity and density. *J Biomech* 1988; 21:13-16.
30. Loder RT: Skull thickness and halo-pin placement in children: the effects of race, gender, and laterality. *J Pediatr Orthop* 1996;16:340-343.
31. Marcus JR, Domeshek LF, Loyd AM, Schoenleber JM, Das RR, Nightingale RW: Use of a three-dimensional, normative database of pediatric craniofacial morphology for modern anthropometric analysis. *Plast Reconstr Surg* 2009;124:2076-2084.
32. Roth S, Vappou J, Raul JS, Willinger R: Child head injury criteria investigation through numerical simulation of real-world trauma. *Computer methods and programs in biomedicine*, vol 93/1. 32-45. 2009; Roth S, Raul JS, Willinger R. Finite element modelling of paediatric head impact: Global validation against experimental data. *Computer Methods and Programs in Biomedicine* 2010;99(1): 25-33.

## 6. Discussion and Outlook

### 6.1 Discussion

Interest in medical applications of lasers, especially as surgical alternatives, has considerably increased due to distinct laser-related advantages, such as non-contact intervention, less trauma, minimal invasiveness, and less heat damage, particularly in the field of oral and maxillofacial surgery. The scope of this dissertation was, based on the methods of computer-assisted and robot-assisted surgery, to design the complete workflow for the assessment of the usability and the effectiveness of a computer-assisted and robot-guided laser osteotome. In-vivo animal and human cadaver experiments were performed to evaluate its performance before the system can be considered for clinical use. Development of the prototype went hand-in-hand with the clinical implementations, thanks to close collaboration between clinicians and engineers.

Currently, most industrial laser applications already make computer- and robot-assisted laser cuts, while for medical and dental purposes, the laser source is used manually (1). However, the methods used for different material processing in industrial settings are not adoptable for medical use as the patient represents an imprecise workpiece owing to considerable inter-individual variability with respect to anatomy and pathology. Additionally, the medical and industrial fields have entirely different requirements; above all, the driving principle of surgical robotics is not to increase productivity but to enhance precision. Ever since the development of the first laser, researchers have assessed their use for cutting bony tissue (2). Studies identified suitable wavelengths in the infrared range, which exhibits good absorption by hydroxyapatite or water in the bone (3). At the beginning of laser use, the most propagated laser source was the CO<sub>2</sub> laser (4). However, the use of this laser source was not straight forward as it induced thermal damage via bony tissue carbonization (5,6). Studies conducted using Er:YAG laser sources around the 1990s demonstrated that laser pulse durations between 100 and 500  $\mu$ s were below the thermal relaxation time so that hard tissue ablation was possible (7–9). For the ablation process to be effective and spare the surrounding tissue, fast energy deposition is required. It is necessary to guarantee that the internal pressure build-up is faster than the diffusion of heat. Only then, will the main part of the deposited energy be used for ablation through micro-explosions after which the heat will leave the tissue together with the ejected tissue particles (debris) and vapor. It is obvious that ablation efficiency directly influences thermal side effects. The erbium laser was the first that achieved good outcomes



for dental medicine and was cleared by the United States Food and Drug Administration for use in cutting human teeth and jaw bones in vivo (10).

Our prototype uses a flash-pumped, solid crystal active laser medium of yttrium aluminum garnet doped with erbium with a pulse duration of 200  $\mu\text{s}$  and a cutting width of 0.5 mm. The laser operates at a wavelength of 2.94  $\mu\text{m}$ . Of all infrared lasers, the erbium laser wavelength of 2.94  $\mu\text{m}$  has the highest absorption in water and hydroxyapatite and is thus optimal for optical drilling (11). The mechanism of action implies that the energy released by each laser pulse creates a micro-explosion within the targeted tissue, leading to immediate release of the targeted material before diffusion of heat into surrounding tissues is possible. Laser energy is primarily transformed into kinetic energy, and since the released materials follow the path of least resistance, they are ejected and leave the ablated site free of debris. This is in opposition to the “smear layer” and the impaction of debris that is observed when using mechanical- and ultrasound piezosurgery-osteotome. From this quantity of heat, only a small part remains in the tissue adjacent to the beam path. However, this heat accumulates if subsequent pulses by the laser beam target the same spot. Three CARLO<sup>®</sup> functions primarily prevent tissue overheating:

- (1) Because ablation occurs only during short periods of time during a laser pulse and because the power of the laser beam is much higher in its center than in its periphery, the heat peak in the illuminated tissue is expelled into debris. This action removes energy in the form of evacuated heated materials and kinetic energy so that heat does not have enough time to diffuse into the tissue. The tissue relaxation time is respected.
- (2) The laser beam sweeps systematically along the pre-operatively-defined osteotomy path at a defined speed while maintaining a consistent overlap between consecutive laser pulses. This continuous motion contributes to limitations of the amount of energy delivered at a given location.
- 3) A water-cooling system was designed to remove the remaining heat in the bone until the next laser pulse comes. The water spray maintains moisture in the targeted tissue to ensure that the ablation properties of the bone and thermal conductivity remain constant within the limits of the entire ablation process. Wet-lab tests with an infrared thermal camera confirmed that the temperature of the bone adjacent to the osteotomy site did not exceed the critical threshold temperature of 45 °C at which prolonged exposure is known to cause irreversible changes in the remaining tissue.

Thirdly, a water-cooling system has been designed to remove the remaining heat in the bone until the next laser pulse comes. The water spray keeps the targeted tissue moistured to ensure that the ablation properties of the bone and the thermal conductivity remain constant respectively within limits during the entire ablation process. Wet-lab tests with an infrared thermal camera confirmed that the temperature of the bone adjacent to the osteotomy site did not exceed the critical threshold temperature of 45 °C at which a prolonged exposure is known to cause irreversible changes in the remaining tissue.

The first goal using this tool was an in-vivo experiment in sheep to check whether our selected laser parameters enabled bone cutting and to assess wound healing in comparison to that achieved with a piezoelectric osteotome (the standard tool for osteotomies in cranio-maxillofacial surgery). A sheep model was used because it closely mimics bone metabolism in humans. At eight post-operative weeks, all bone samples from the laser and piezo groups showed good healing with no signs of complications or carbonization; however, laser osteotomy was associated with accelerated healing, as assessed by histological examination and micro-CT analysis. Besides, the laser group exhibited a symmetric cutting pattern and constant osteotomy depth and therefore an improved accuracy in maintaining of the planned geometries compared to the piezo-osteotome. Better bone healing after laser osteotomy has been already demonstrated in several previous studies (12-14). Thus, the first step of this thesis proved enhanced bone healing after Er:YAG laser cuts and represented an important milestone for further application of the prototype. If a biostimulating effect of Er:YAG, as described by Pourzarandian et al. (15), had occurred, it was not investigated. This group reported that both prostaglandin E2 (PGE2) and Er:YAG laser irradiation accelerate wound healing. The stimulatory action of the laser seems to occur during the proliferative stage of healing via stimulation of PGE2 and cyclooxygenase-2 (COX-2), which are crucial early mediators in the natural healing process. PGE2 and COX-2 gene expression in human gingival fibroblasts after Er:YAG laser tissue exposure in vitro was examined. They described how the Er:YAG laser significantly increased PGE2 production by human gingival fibroblasts. COX-2 mRNA, which was hardly detectable in the control, increased significantly after irradiation. The results of Pourzarandian et al. showed that Er:YAG laser irradiation appears to exert its stimulating action on gingival fibroblast proliferation through PGE2 production via the expression of COX-2. These authors stated this should be considered as one of the important regulatory pathways to accelerate wound healing after Er:YAG laser irradiation. In this thesis this phenomenon was not investigated but should be a starting point for further investigations.

In a next step, a representative dummy operating room wet lab and subsequent human cadaver study, which was used as the proof of concept for the ergonomic setup of the prototype

and the demonstration of the feasibility of its use. A series of representative surgical indications in the maxillofacial field were used for evaluation of the possible cutting depth. Reconstruction of a mandible defect with a free fibula flap was simulated. Both investigations demonstrated that cold-ablation and a robot-guided laser osteotome can be easily integrated into the instrumental setup of an operation theater. From a trolley position close to the head of the patient, all surgical sites for the majority of cranio-maxillofacial indications can be reached by the robotic arm with a diameter range of 790 mm in a stretched position. Collision free execution and reachability are particularly important issues for this type of surgery. The compact construction and positioning of the laser head at the tool center point of the robotic arm provided enough space for the surgeon and his assistant to perform the intervention. With the chosen laser parameters, 2.3 cm of bone depth could be attained with no signs of carbonization on the cutting surface. For navigation applications, the relevant working volume was achieved within a distance range of 1.5 to 2.0 m. The firmware of the tracking camera supported optical markers with 3 to 4 fiducials. With this system, the three-dimensional (3D) orientation of several optical markers (both active and passive) could be concurrently measured. The overall resulting 3D tracking accuracy was approximately 0.09 mm RMS. The registration process (matching CT scans and planning data consisting of *in situ* measurements) showed a precision level comparable to that achieved with the existing navigation systems. The reached RMS errors averaged 0.818 mm and ranged from 0.257 to 1.311 mm. These outcomes were consistent with published results from other navigation systems used in cranio-maxillofacial surgery.

In addition to the navigation system, the CARLO workflow provided visual accuracy control for the surgeon prior to each execution of the laser during the osteotomy. A visible green laser light indicates the predicted cutting path, allowing for verification of the correctness of the planned osteotomy. Throughout all of the tested osteotomies in this PhD project, it could be confirmed that the cut path was satisfactorily mapped onto the specimen's bone. The registration time in the cadaver study (average: just over 8 min; range, 405–1343 sec) is also acceptable for clinical use given that the surgical procedures typically involve several hours.

In summary, the key results of the human cadaver study are shown below:

1. The confirmation of the usability of the CARLO® software and the complete workflow, from the planning of osteotomies based on preoperative CT scan images, to the osteotomy implementations.
2. Confirmation of the performance of the navigation system: in particular, the procedures confirmed that the targeted largest registration RMS error of  $\leq 1.5$  mm could consistently

be achieved in a few minutes and that the planned osteotomies could precisely be performed.

3. No macroscopically visible thermal alteration could be observed on the bone cut surfaces in the prototype group.
4. To the best of our knowledge, a 2.3 cm of ablation bone depth was reached for the first time using a laser cut.
5. No unwanted collision of the device occurred during all tests. Overall, no safety problems arose.

For the above-mentioned tests, our prototype underwent some modifications. The in-vivo sheep trial was conducted using an off-the-shelf laser source, taken from the LiteTouch medical device (Syneron®), while modifying the optics and cooling to accommodate the working distance appropriate for a robot. For the cadaver studies, a custom-built laser source allowed increased uniformity of the beam to be achieved. During the initial tests, bone ablation parameters were set with a similar overall power level to those suggested by the manufacturer. With 400 mJ and 10 Hz, a power of 4.0 W was reached. A pulse rate of 10 Hz was found to be appropriate for allowing systematic robotic motion between consecutive pulses. For the cadaver test, the laser parameters were modified to enable a 40 % increase of the delivered power. This improvement was associated with a more uniform distribution of the beam energy within the focal area, and an increased focal distance allowing maintaining a safe working distance of 80 mm between the robot-driven laser head and the targeted tissue. The pulse width was also modified from 250  $\mu$ s in the animal investigation to 200  $\mu$ s in the human cadaver study to ensure that cold ablation occurred in order to minimize residual heat transfer to the surrounding tissue. Therefore, the targeted tissue should remain humid and covered by a film of water solution. However, a larger volume of delivered saline solution did not improve cooling.

On the contrary, an excess of saline solution can drain from the tissue and smear the surgical field leading to a condition that is clinically undesirable. Accordingly, a fine mist of small droplets was delivered by spray nozzles. A reduction from 33 ml/min to a fine mist of 8 ml/min for the cadaver trials was done. With this shift of the cooling parameters, optimal tissue cooling (no carbonization) and a greater surface for evaporation could be achieved. The effect seemed to contribute to the efficacy of the ablation process.

Complex and freely selectable cutting geometries with laser photo-ablation are feasible (13). This type of cutting opens new possibilities for removal of bony tissue due to a considerably smaller cutting diameter of 500  $\mu$ m and thus, reduced bone loss. In comparison, mechanical- and ultrasound-driven osteotomy tools have a greater diameter nowadays. The thinnest of these tools is the piezo-osteotome with a tip width of 0.6 mm. Through the narrow

bone incision width and specific osteotomy design, a self-stabilizing, macro-retentive osteotomy geometry is possible. Among other cut geometries, in the cadaver study, dovetail-like patterns for the mandible resection were selected. These functional cuts led to a simplified reconstruction situation of the defect with a corresponding cut in the fibula graft. Thanks to these interlocking surfaces of bone, increased primary stabilization and a load-bearing situation followed, which allowed minimization of the amount of osteosynthesis material to be used. It might even be possible to use resorbable materials instead of metal implants. Biomechanical studies are needed to verify this statement. Another advantage of using this technique is the omission of a cutting guide/template for the fibula graft osteotomy and the turnaround time for preparing the tool for upcoming interventions due to its contactless cutting mechanism. Besides the costs for the cutting templates, this technique might even render a less accurate outcome than the laser due to possible planning failures, fabrication errors, faulty template positioning during the operation, and/or inadequate representation of the anatomy in the planning steps.

The possibility to realize complex cutting geometries is an advantage in the correction of highly demanding 3D procedures as seen, for example, in craniosynostosis-affected children. Craniosynostosis is a relatively rare congenital malformation of the skull, resulting from the premature fusion of one or more cranial sutures. In normal development, cranial growth occurs perpendicular to the suture lines and leads to a well-proportioned head with a longer anteroposterior than bitemporal dimension. Premature fusion of one or more sutures precludes the growth of cranial bones perpendicular to the affected sutures and leads to compensatory growth in a parallel direction, resulting in a cranial dysmorphic head shape. The main purpose of the correction of a craniosynostosis skull is to re-open the cranial sutures with bone slots to free the skull bones and allow proper internal brain development. The surgical correction of craniosynostosis is complex. As early surgery is beneficial, there is a demand for less invasive but effective techniques because the correction presents a time-consuming and complex challenge. The difficulty with correction relates to proper positioning of the bone flaps. To enfeeble the flap in a determined form is still a challenge. As bone in children between one and two years is more brittle, bending is less effective. Thereby, the usual osteotomy of the cranial vault leaves defects between the bone segments that tend to be larger at this age. These children usually require bone grafting. Therefore, for an ideal cutting pattern, attention must be paid to the depth. If the depth is not sufficient, early osseous healing would result in a new skull deformation again with possible increased intracranial pressure. On the contrary, if the cut is too deep, the development of permanent bone defects with the risk of cerebral impairment exists. Both conditions would result in secondary surgery with additional morbidity for the patient. Consequently, there is a wide agreement that preoperative planning is

unavoidable. Current planning systems (16,17) allow an iterative sequence of osteotomies and repositioning trials for the optimal reconstruction plan. Nowadays, the inner layer of the bone flaps is not osteotomized so that the flap deformations, even if preoperatively planned, are more randomly forming a drawback in terms of precision. The usual flap repositioning of the cranial vault leaves defects between the bone segments that tend to be larger if the affected child is elder. These patients consecutively require bone grafting. The question is whether an internal osteotomy with predefined patterns enfeebls the bone in a way that it can be deformed with an optimal stress distribution and an enlargement of the flap surface. Virtual planning tools combined with robot-guided laser osteotomy offer major advantages in these corrective procedures in relation to bone healing time, reduced bone loss, and direct connection of the virtual plan to the laser osteotome without intermediate devices, such as bone surface or cutting guides. Therefore, in the last part of this doctoral thesis, the influence of different cutting geometries in the field of craniosynostosis correction was evaluated. The relationship between various possibilities of bone osteotomies and skull rigidity was examined. For this purpose, finite element analysis methods were used to create spherical bone model according to a frontal bone segment. The different deformation responses to different cutting patterns on the inner layer were investigated. In particular, the best-suited cutting geometry and precise location of these cuts on the inner layer of the bone flap was determined to allow the optimal “moldable bone”. The objective was to obtain enough evidence to select the best cutting pattern according to the degree of skull deformation. Our results demonstrated an optimal osteotomy pattern that required only a low force to bend the bone samples and resulted in better stress distribution thus achieving optimal molding characteristics while maintaining reasonable stability of the bone flap. With the selected pattern parameters, an over expansion of the surface of 20.7% could be achieved. Even if virtual models allow better visualization of the problem, these suppositions must be further evaluated in cadaver skull studies.

Automatized laser bone ablation is suitable for assuming a major role in bone surgery. The focus of this PhD thesis was to describe the development and evaluation of preclinical methods for cold-ablation and robot-assisted laser osteotomy for the first time. The entire system was designed to maximize the benefits of contact-free laser cutting while ensuring the usability for surgeons and safety for surgeons and patients. The investigations demonstrated the clinical applicability of this prototype for performing osteotomies with high precision according to preoperative 3D planning of complex incisions trajectories and individual patient-designed osteotomy patterns. The outcomes reached a level of accuracy unachievable by manually guided laser devices, either with or without the support of a navigation system. Considering

the state-of-the-art systems, this was inconceivable up to now. Additionally, the results present the possibility for faster bone healing compared to the piezoelectric osteotome as the state-of-the-art osteotomy device. In summary, the cold-ablation and robot-guided Er:YAG laser osteotome, called CARLO<sup>®</sup>, already offers effectiveness and applicability for bone removal into the next era.

## 6.2 Outlook

The contributions of this doctoral thesis raises two further main scientific questions, which are essential to investigate before applying the robot-guided laser osteotome. On one hand, this investigation addresses concepts for online measurement of the ablation process, and on the other hand, it addresses improvements in laser parameters to allow ablation speeds comparable at least to the ultrasound driven piezoelectric osteotome to be reached.

In order to ablate safety bone containing critical boundaries, such as nerves, dura mater at the skull, or blood vessels, depth control is the key prerequisite for any cutting tool. This control is even more critical for robot-guided laser osteotomy in which surgeons have no direct control over the cutting process due to the lack of haptic feedback. Therefore, it is only possible to control bone removal visually. In this context, optical coherence tomography (OCT) offers promising potential. In this regard, the paper of Fuchs et al. (18) presents an automatic depth control pathway in bone ablation through a closed-loop control based on OCT data. The study was based on combined working volumes of OCT and an Er:YAG cutting laser. The original bone surface was derived from an initially acquired 3D OCT scan. Afterwards, the iterative control cycle consisted of image processing, path planning, bone ablation of the targeted geometry, and desired cavity depth on fresh porcine bone samples of  $3 \times 3 \times 1 \text{ mm}^3$ . Using a mathematical model, the theoretical cavity depth was calculated for each laser pulse and displayed on the navigation screen. Thereby, the material removal was determined in a volumetric model. The results showed promising outcomes with high precision of the ablation process with mean values of depth of 0.96 mm, width of 2.87 mm, and length of 2.82 mm.. In the first study of this thesis, OCT software was integrated in the ablation control loop to map the targeted bone ablation depth for each location in real-time in the animal study. In the optical spectrum, a strong back-reflection from the sample arm fiber end was detected, depending on the length of the reference arm. Therefore, due to scanning errors during acquisition, the results were unfortunately not representative and not further assessed. Definitively solving this problem is required. After that improvement, the performance of the long-range OCT depth control system along the z-axis (laser beam axis) opens the possibility for use of this system in providing real-time measurements of both cutting depths and profiles. Other improvements include calibration of the OCT to account for the presence of water vapor or other transparent media and addition of a depth sensor based on the photoacoustic spectroscopy effect to complement these measurements and thus increase safety. All of these tasks must be examined in future studies. Promising results with an OCT system have already been reported by Mohebbi et al. (15). In this feasibility study, the OCT system was used for laser marking of the border of the internal auditory canal with an overall accuracy of 300  $\mu\text{m}$ . Important in this



system is consideration of the different structures of bone, such as cortical versus spongiform, which can result in different ablation amounts. To sense the depth of the photoablation, the prototype software should offer the possibility to calculate the depth using a theoretical value. With the knowledge of the bone thickness of the osteotomy path in the region of interest based on the preoperative CT scan and knowledge of the ablation rate per laser pulse, (such as 400 to 500  $\mu\text{m}$ ), the number of required pulses can be calculated.

The main drawback of laser ablation, especially in comparison with mechanical cutting instruments, is its relatively low processing and cutting speed. By variation and adjustment of the laser parameters in addition to bone composition influences the amount of bone removed by a single laser pulse. Obviously, thermal dispersion should also be taken into consideration. By changing the laser parameters in different preclinical examinations, the velocity of the ablated bone volume at the focus point per pulse could be improved from 5 to 10  $\text{mm}^3/\text{s}$ . In the cadaver trials, equivalent ablation rates were achieved as seen with the piezo-osteotome. In industrial applications, femtosecond short-pulsed and high energetic lasers are now being used for material cutting. With optimal conditions of the laser parameters, studies demonstrated that the overall processing speed was more than four times faster than the maximum reported previously (19,20). Ultrashort pulse durations deliver extremely high peak power, resulting in a multiphoton absorption. This mechanism opens up new possibilities for machining of materials that are not dependent on the single photon absorption properties of the material. The main benefit of ultrafast laser machining lies in the strongly non-thermal nature of the ultrafast process. The pulse durations are smaller than the thermal diffusion time. Hence, femtosecond lasers are not suitable for bone surgery purposes. Due to the high peak power, carbonization of the wound boundaries with impairment of healing would result. So far, no method has been shown to increase processing speed without negatively affecting bone healing. Further developments in laser technology and adjustment of laser parameters may help optimize the cutting speed. However, CARLO<sup>®</sup> offers advantages over the current state-of-the-art cutting tools, such as less bone loss, precise and real-time navigated execution of predefined geometries, free osteotomy patterns, and higher primary stability due to precise fitting of the graft.

Finally, after undergoing extensive development and design evolutions, to improve usability and safety, and to achieve compliance with essential requirements and applicable standards, efforts to introduce the prototype in clinical settings are already underway. A multicenter study is envisaged to perform midfacial osteotomies using a transoral approach. This would enable useful clinical experiences with CARLO<sup>®</sup>.

## 6.3 Literature

- 1 Nishimoto S, Tsumano T, Kawai K, Ishise H, Kakibuchi M, Shimokita R, Yamauchi T, Okihara S. The dawn of computer-assisted robotic osteotomy with ytterbium-doped fiber laser. *Lasers Med Sci.* 2014;29:1125-9
- 2 Verschueren RC, Koudstaal J, Oldhoff J. The carbon dioxide laser; some possibilities in surgery. *Acta Chir Belg.* 1975;74(2):197-204
- 3 Nagy Abdulsamee. Erbium Family Laser: Silent Revolution in Dentistry. Review. *EC Dental Science.* 2017;13:168-190
- 4 Schmidt B, Kránicz J, Montskó P, Novák L. The use of CO<sub>2</sub> laser in bone surgery. *Magy Traumatol Orthop Helyreallito Seb.* 1991;34:331-6
- 5 Rayan GM, Pitha JV, Edwards JS, Everett RB. Effects of CO<sub>2</sub> laser beam on cortical bone. *Lasers Surg Med.* 1991;11(1):58-61
- 6 Kuttenger JJ, Waibel A, Stübinger S, Werner M, Klasing M, Ivanenko M, Hering P, von Rechenberg B, Sader R, Zeilhofer HF. Bone healing of the sheep tibia shaft after carbon dioxide laser osteotomy: histological results. *Lasers Med Sci.* 2010;25:239-249
- 7 Hibst R: Mechanical effects of erbium:YAG laser bone ablation. *Lasers Surg Med* 1992;12:125-130
- 8 Akyol UK, Guengoermues M, Guendogdu C, Erdem H: Histologic evaluation of the effects of Er: YAG laser on bone ablation. *J Contemp Dent Pract* 2009;10:65-72
- 9 Sasaki KM, Aoki A, Ichinose S, Yoshino T, Yamada S, Ishikawa I. Scanning electron microscopy and Fourier transformed infrared spectroscopy analysis of bone removal using Er:YAG and CO<sub>2</sub> lasers. *J Periodontol.* 2002;73(6):643-52
- 10 Cozcan C, Arcoria CJ, Pelagalli J, Powell GL. Dentistry for the 21<sup>st</sup> century? Erbium:YAG laser for teeth. *J Am Dent Ass.* 1997;128:1080-1087
- 11 Lukac, M, Marincek M, Grad L. Dental laser drilling: Achieving optimum ablation with the latest generation Fidelis laser systems. *J Laser Health Acad.* 2007;7:1-4
- 12 Lewandowski KU, Lorente C, Schomacker KT, Flotte TJ, Wilkes JW, Deutsch TF. Use of the Er:YAG laser for improved plating in maxillofacial surgery: comparison of bone healing in laser and drill osteotomies. *Lasers Surg Med.* 1996;19(1):40-5
- 13 O'Donnell RJ, Deutsch TF, Flotte RJ, Lorente CA, Tomford WW, Mankin HJ, Schomacker KT. Effect of Er:YAG laser holes on osteoinduction in demineralized rat calvarial allografts. *J Orthop Res.* 1996;14(1):108-13
- 14 Pourzarandian A, Watanabe H, Aoki A, Ichinose S, Sasaki KM, Nitta H, Ishikawa I. Histological and TEM examination of early stages of bone healing after Er:YAG laser irradiation. *Photomed Laser Surg.* 2004;22(4):342-50

- 15 Pourzarandian. A, Watanabe H, Ruwanpura SM, Aoki A, Noguchi K, Ishikawa IEr:YAG laser irradiation increases prostaglandin E production via the induction of cyclooxygenase-2 mRNA in human gingival fibroblasts. *J Periodontal Res.* 2005;40:182-186
- 16 Tolhuisen ML, de Jong GA, van Damme RJM, van der Heijden F, Delye HHK. Cranial shape comparison for automated objective 3D craniostosis surgery planning. *Nature.* 2018;8:3349-3356
- 17 Jans G, van der Sloten J, Gobin R, van der Perre G, vand Audekercke R, Mommaerts M. Computer-aided craniofacial surgical planning implemented in CAD-software. *Comput Aided Surg.* 1999;4:117-128
- 18 Fuchs A, Pengel S, Bergmeier J, Kahrs LA, Ortmaier T. Fast and automatic depth control of iterative bone ablation base on optical coherence tomography data. 2015; *Proceedings of SPIE 9542*; doi.org/10.15488/2548
- 19 Mohebbi S, Lexow J, Fuchs A, Rau T, Tauscher S, Mirsalehi M, Sadr Hosseini SM, Ortmaier T, Lenarz T, Majdani O. Feasibility Assessment of Optical Coherence Tomography-Guided Laser Labeling in Middle Cranial Fossa Approach. *Iran J Otorhinolaryngol.* 2018;30(101):321-327
- 20 Wang XC, Zheng HY, Chu PL, Tan KM, Liu T, Bryden CY, Tay GH. High quality femtosecond laser cutting of alumina substrates. *Optics Lasers Engineering.* 2010;48:657-663
- 21 Oosterbeek RN, Ward T, Ashforth S, Bodley O, Rodda AE, Simpson MC. Fast femtosecond laser ablation for efficient cutting of sintered alumina subtrates. *Optics Lasers Engineering.* 2016;84:105-110

## 7. List of publications on PhD topic

### 7.1 Peer-reviewed Journal publications

Juergens P, **Augello M**, Baek K, Deibel W, Baetscher C, Segesser M, Cattin P, Zeilhofer HF. Execution of midfacial osteotomies with a cold ablation robot-guided laser osteotome. *Int J Oral and Maxillofacial Surgery* 2017 46 (1); 205

Deibel W, Schneider A, **Augello M**, Bruno A, Juergens P, Cattin P. A compact, efficient and light weight laser head for CARLO®: Integration, performance and benefits. *Proceedings of SPIE*. 2017.

<http://spie.org/Publications/Proceedings/Paper/10.1117/12.2187992>

**Augello M**, Deibel W, Nuss K, Cattin P, Jürgens P: Comparative microstructural analysis of bone osteotomies after cutting by computer-assisted robot-guided laser osteotome and piezoelectric osteotome: an in vivo animal study. *Lasers Med Sci*. 2018 Sep;33(7):1471-1478

**Augello M**, Baetscher C, Segesser M, Zeilhofer HF, Cattin P, Juergens P. Performing partial mandibular resection, fibula free flap reconstruction and midfacial osteotomies with a cold ablation and robot-guided Er:YAG laser osteotome (CARLO®) - A study on applicability and effectiveness in human cadavers. *J Cranio Maxfac Surg*, 2018 Oct;46(10):1850-1855

**Augello M**, Maurer M, Berg-Boerner I, Zeilhofer HF, Cattin P, Juergens P. The use of FEM analysis for modeling different osteotomy patterns and biomechanical analysis of craniosynostosis treatment. *J Craniofacial Surgery*, 2019, doi: 10.1097/SCS.00000000000005579

Berg-Boerner I, Peyer M, **Augello M**, Kuske L, Steineck M, Deibel W, Mathys W, Jürgens P, Kunz, Goldblum D. Comparison of an Er: YAG Laser Osteotome Versus a Conventional Drill for the Use in Osteo- Odonto-Keratoprosthesis (OOKP). *Lasers Surg Med*, 2019 Jan;15: doi: 10.1002/lsm.23053

## 7.2 Oral presentations

### 2018

- 24th Congress of the European Association for Cranio Maxillo Facial Surgery (Munich, D): „The new frontier of robot-assisted surgery for maxillofacial osteotomies “

### 2017

- 20. Annual Congress of the Italian Society of Oral- and Maxillofacial Surgery (Neapel, I): “CARLO – Un robot che rivoluzionerà la chirurgia maxillofacciale”, Invited Speaker.
- Congress for advanced digital technology in head & neck reconstruction (Amiens, F): “Preclinical evaluation of cold ablation and robot-guided laser osteotome to perform parietal craniotomies in sheep and a first cadaver trial for Le Fort I and mandible resection with functional cutting pattern.”

### 2016

- Int. Symposium for Cranio Maxillo Facial Surgery (St. Anton, A): „Ist die automatisierte Roboter-geführte Laserosteotomie bereit für den klinischen Einsatz?“
- Annual Kongress of the Swiss Society of Oral and Maxillofacial Surgery (Solothurn, CH): „Roboter-geführtes Knochenschneiden. Nur eine Zukunftsvision?“
- Annual Congress of the German Society of Oral and Maxillofacial Surgery (Hamburg, D): „Präklinische Evaluation eines Computer-assistierte und Roboter-geführten Laserosteotoms im Tierversuch“

## **7.3 Posters**

### **2018**

- Research day of the Department of Surgery, University Hospital Basel: „Performing partial mandibular resection, fibula free flap reconstruction and midfacial osteotomies with a cold ablation and robot-guided Er:YAG laser osteotome (CARLO®). A study on applicability and effectiveness in human cadavers.

### **2017**

- 20. Annual Congress of the Italian Society of Oral and Maxillofacial Surgery (Naples, I): La rivoluzione nel campo maxilla-facciale con CARLO®.”

### **2016**

- Research day of the Department of Surgery, University Hospital Basel: „Preclinical evaluation of a computer-assisted and robot-guided laser-osteotomy tool to perform osteotomies in an animal study.”
- 14. International Bernd Spiessl Symposium: Face and Identity Basel: „Bone surgery innovation? An autonomous working laser osteotome – CARLO®.”

### **2015**

- “Cells & Materials Meeting Lausanne: „Using a Computer-Assisted and Robot-guided Laser Osteotome (CARLO®) in bone surgery - considerations on ergonomics, system accuracy and biological response.”

## 8. Curriculum vitae

Marcello Augello

Dr. med. Dr. med. dent. (MD, DDS)

Specialist for Cranio-Maxillofacial Surgery FMH, EBOMFS

Specialist for Oral Surgery SSO

Family Physician FMH

Ability Certification for Neck Ultrasound SGUM

### Education

1990 - 1995	High school Frauenfeld, Degree in economics
1995 - 2000	Dentistry studies University Zurich
2001 - 2004	Human medicine studies University Zurich
2004	Promotion DMD
2004 - 2005	Medical assistant Surgical Clinic Kantonsspital Frauenfeld (Dr. med. K.Oehy
2005 - 2009	Medical assistant Cranio-Maxillofacial Surgery University Hospital Zurich and Clinic for Oral Surgery (Prof. Dr. Dr. med. K. W. Grätz) Anesthesiology Kantonsspital Münsterlingen (PD Dr. med. Th. Neff)
2010	Promotion MD
2010	Specialist of Dental Surgery SSO
2011	Praktischer Arzt, Specialist family physician FMH
2011	Medical assistant Cranio-Maxillofacial Surgery Johannes Wesling Klinikum Minden (PD Dr. med. W. Engelke)
2011 - 2017	Medical assistant Clinic for Cranio-Maxillofacial Surgery University Hospital Basel (Prof. Dr. Dr. med. Dr. h. c. H.-F. Zeilhofer)
2013	Specialist in Cranio-Maxillofacial Surgery FMH
2014	PhD Program Profs. Jürgens and Cattin
2015 - dato	Senior Consultant Department of Cranio-Maxillofacial Surgery Kantonsspital Aarau
2016	Specialist for Neck Ultrasound, SGUM
2016	Fellow of the European Board of Oro-Maxillo-Facial Surgery Head and Neck
2017	Fellow Deutsche Gesellschaft für ästhetische Botulinum- und Fillertherapie e.V.
2018	Fellow Network-Globalhealth für Lypolyse und ästhetische Medizin